The Viral SUMO−Targeted Ubiquitin Ligase ICP0 is Phosphorylated and Activated by Host Kinase Chk2

Dambarudhar Shiba Sankar Hembram [1], Hitendra Negi [1,2], Poulomi Biswas [1,†], Vasvi Tripathi [1], Lokesh Bhushan [1], Divya Shet [1,‡], Vikas Kumar [1,§] and Ranabir Das [1]

1 - National Center for Biological Sciences, *TIFR, Bangalore, India*
2 - SASTRA University, *Thirumalaisamudram, Thanjavur, India*

Correspondence to Ranabir Das: *rana@ncbs.res.in*
https://doi.org/10.1016/j.jmb.2020.01.021
Edited by Titia Sixma

Abstract

When the herpes simplex virus (HSV) genome enters the nucleus for replication and transcription, phase-segregated nuclear protein bodies called Promyelocytic leukemia protein nuclear bodies (PML NBs) colocalize with the genome and repress it. HSV encodes a small ubiquitin-like modifier (SUMO)−targeted ubiquitin ligase (STUbL) infected cell polypeptide 0 (ICP0) that degrades PML NBs to alleviate the repression. The molecular details of the mechanism used by ICP0 to target PML NBs are unclear. Here, we identify a bona fide SUMO-interacting motif in ICP0 (SIM-like sequence [SLS] 4) that is essential and sufficient to target SUMOylated proteins in PML NBs such as the PML and Sp100. We shown that phosphorylation of SLS4 creates new salt bridges between SUMO and SLS4, increases the SUMO/SLS4 affinity, and switches ICP0 into a potent STUbL. HSV activates the Ataxia−telangiectasia-mutated kinase-Checkpoint kinase 2 (ATM-Chk2) pathway to regulate the cell cycle of the host. We report that the activated Chk2 also phosphorylates ICP0 at SLS4 and enhances its STUbL activity. Our results uncover that a viral STUbL counters antiviral response by exploiting an unprecedented cross-talk of three post-translational modifications: ubiquitination, SUMOylation, and phosphorylation.

Introduction

DNA viruses optimize the host nuclear environment for genome replication and transcription. Promyelocytic leukemia protein nuclear bodies (PML NBs, also known as ND10 or PODs) are dynamic nuclear substructures located in the interchromosomal space. These multiprotein phase-segregated bodies serve as an antiviral response to prevent transcription of viral genes during infection [1−4]. In the nucleus, the incoming viral genome triggers the spontaneous formation of PML NBs around it, which transcriptionally represses the genome[5,6]. PML NBs inhibit the growth of several viruses, including the entire Herpesviridae family, adenovirus, papovavirus SV40, papovavirus adeno-associated virus (AAV), and polyomavirus [7]. Viruses counteract by disrupting and degrading the PML NBs [8]. Herpes simplex virus-1 (HSV-1) expresses an ubiquitin ligase (E3) known as the infected cell polypeptide 0 (ICP0) in the immediate early stages of the lytic cycle [9]. A prominent role of ICP0 is to degrade PML NBs via the ubiquitin-proteasome pathway [10,11]. ICP0 is a Really New Interesting (RING) finger E3, and its catalytic RING finger domain is essential for the degradation of PML NBs [12]. ICP0-deleted HSV-1 fails to degrade PML NBs, resulting in reduced viral gene expression [9,13]. These results suggest that the degradation of PML NBs is imperative for HSV-1, and ICP0 is indispensable for this purpose.

Interestingly, another member of the ubiquitin family, the small ubiquitin-like modifier (SUMO), is also involved in this process. The essential constituent proteins of PML NBs such as PML, hDaxx, and Sp100 are heavily SUMOylated, and ICP0 targets them to disrupt PML NBs [3]. E3s that target SUMOylated substrates are known as SUMO-targeted ubiquitin ligases (STUbLs)[14]. Apart from the catalytic RING finger domain, STUbLs contain

SUMO-interacting motifs (SIMs), which bind to SUMOylated substrates and enable the E3 to assemble polyubiquitin chains on the substrates. Recent investigations indicate that indeed ICP0 is a viral STUbL, which recognizes the SUMOylated proteins by one or more of its seven predicted SIM-like sequences (SLS1-7) [15,16]. However, the identity of the bona fide SIMs in ICP0 and the molecular details of how ICP0 targets SUMOylated substrates remain elusive. Intriguingly, PML NBs are short-lived after ICP0 expression, indicating that they undergo rapid degradation because of ICP0. The same is true for the PML NBs observed in HSV-1−infected cells. However, typical SUMO/SIM interactions are weak, with dissociation constants about 100 μM [17]. It is unclear how ICP0 can efficiently target SUMOylated substrates for rapid degradation, despite the weak SUMO/SIM interaction.

HSV-1 activates the ATM-Chk2 pathway to arrest cells in the G2/M phase and promote virus growth. Expression of ICP0 triggers a series of phosphorylation events resulting in activation of ATM, Chk2, cytoplasmic sequestration of Cdc25C, and CDK1 inactivation resulting in G2/M arrest [18]. Although the pathway is initiated by the activation of ATM, any further interaction between ICP0 and the downstream factors in the ATM-Chk2 pathway is unknown. However, ICP0 and Chk2 transiently colocalize at the PML NBs [19]. Whether ICP0 and Chk2 can directly interact and any molecular details of such interaction are unclear. In addition, whether the activation of the ATM-Chk2 pathway provides any further advantages for the HSV-1 infection is unknown.

We carried out a systematic investigation of interactions between SUMO1 and SUMO2 with all the seven predicted SLS regions (SLS1-SLS7) by Nuclear Magnetic Resonance (NMR). We report that SLS4 is the sole bona fide SIM in ICP0. Structural models of the SUMO/SLS4 complexes uncovered a set of hydrophobic and electrostatic contacts between SUMO and SLS4, which are critical for targeting SUMOylated substrates such as PML and Sp100 for ubiquitination. Interestingly, ICP0 ubiquitinates both the SUMO and the substrate in a SUMOylated substrate, suggesting a mechanism that may be crucial to prevent regulation by host deSUMOylating enzymes. Two phosphoserines adjacent to SLS4 are phosphorylated in cellular conditions. Phosphorylation of SLS4 enhances its affinity for SUMO by several folds, increases the ability of ICP0 to target substrates, and switches it into a potent STUbL. Further structural studies revealed molecular details of the interaction between ICP0 and Chk2, which is dependent on the kinase CK1. We further show that CK1 and Chk2 work in tandem to phosphorylate SLS4 and enhance the STUbL activity of ICP0. Besides cell cycle regulation, activated Chk2 also increases the potency of ICP0 to degrade antiviral responses. Altogether, our results demonstrate how a viral E3 exploits the cross-talk of three host post-translational modifications (PTMs), ubiquitination, SUMOylation, and phosphorylation to degrade antiviral responses.

Materials and Methods

Plasmids and peptides

Synthetic genes for SUMO2, ICP0-R, and ICP0-RS4, PML were obtained from Lifetech, which were subsequently cloned in expression vectors. SUMO2 was cloned into pET3a between NdeI and BamHI restriction sites, while ICP0-R, ICP0-RS4, and PML were cloned into pGEX6P-1 between BamHI and NotI sites. The pQE80L-SUMO1 clone was obtained from Dr. Koti, Tata Institute of Fundamental Research, Mumbai. Ube2d1, SUMO-E1, and UBC9 (SUMO-E2) constructs were obtained from Addgene. Chk2-FHA plasmid was a gift from Ashok Venkitaraman (Medical Research Council Cancer unit), and Ube1 plasmid was a gift from Cynthia Wolberger (Johns Hopkins University). SENP2 was a gift from Chris Lima (Memorial Sloan Kettering). Full-length ICP0 was synthesized in a pFastHtb vector (Invitrogen). Mutants of ICP0 were prepared by site-directed mutagenesis. All the synthetic peptides were purchased from Lifetein LLC as lyophilized powders.

Protein expression and purification

All the proteins were expressed in BL21 DE3 either in Luria broth for unlabeled samples or in $^{15}NH_4Cl/^{13}C_6$-glucose M9 media for labeled samples. SUMO1, SUMO2, SUMO-E1, and SUMO-E2 (UBC9) were expressed and purified as discussed earlier [53]. Ube2d1 was purified similar to UBC9. Ube1 and Ub are purified, as discussed earlier [54].

GST-ICP0-R and GST-ICP0-RS4 were cultured at 37 °C to 0.6 OD_{600} and were induced at 18 °C with 1 mM Isopropyl β- d-1-thiogalactopyranoside (IPTG). Cells were lysed by sonication in Phosphate buffer saline (PBS) supplemented with protease inhibitors. The lysate was clarified by centrifugation, and the supernatant was passed through pre-equilibrated Glutathione Agarose (Protino ®) beads for binding. The binding was followed by a high salt wash with 0.5 M NaCl in 50 mM phosphate, 0.1% Triton X-100, and 0.05% sodium azide. Next, the beads were washed with PBS, 0.1% Triton X-100, and 0.05% sodium azide. The protein was eluted with 20 mM reduced glutathione in PBS buffer. Glutathione was subsequently removed by dialysis. GST-PML was purified similar to ICP0-R, except a last step of purification by gel filtration was carried out in PBS.

M9 culture of Chk2-FHA (aa: 64−212) was induced at 18 °C for 16 h. The culture was harvested, and cells were resuspended in 50 mM phosphate buffer with 300 mM NaCl followed by sonication. The supernatant was bound to Ni^{2+} NTA-agarose beads (Protino), washed with 50 mM phosphate, 300 mM NaCl, and 20 mM imidazole buffer. The protein was eluted with 50 mM phosphate and 300 mM NaCl with a gradient of 100~200 mM imidazole.

The purified protein was injected into a gel filtration (Superdex75 16/600 column) equilibrated with 50 mM phosphate, 300 mM NaCl, and 2 mM DTT at pH 7.4.

*Sf*9 cells were grown in 1 × 10 ^{6} for 1 L of Sf900 II (Gibco) media in the presence of antibiotic and antimycotic (Gibco) at 27 °C for 3 days. Fifty milliliter of P3 was added to the *Sf*9 cells to produce full-length ICP0. The cells were incubated for another three days, after which the cells were harvested and lysed in 50 mM Tris-Cl (pH 8.0), 500 mM NaCl, 0.01% tween 20, 2 mM EDTA protease inhibitor (Roche), and 100 mM phenylmethylsulfonyl fluoride (PMSF). The supernatant after centrifugation was purified in by Ni-NTA purification. The final samples were dialyzed in 50 mM Tris-HCl (pH 8.0), 150 mM NaCl, and 2 mM EDTA protease inhibitor (Roche). The mutants of ICP0 were grown and purified in a similar manner as the wt-ICP0.

NMR experiments

The NMR spectra of SUMO1 and SUMO2 were recorded at 298 K on an 800 MHz Bruker Avance III HD spectrometer with a cryoprobe head, processed with NMR pipe [55] and analyzed with Sparky [56]. The SUMO and SUMO/SLS4 NMR samples were prepared in PBS buffer, with 5 mM DTT at pH 7.4 and 10% D_2O. Standard CBCA(CO)NH, HNCACB, HNCA, HN(CO)CA, HNCO, and HN(CA)CO experiments were used for backbone assignments and HCCH-TOCSY for side chain assignments of the SUMO1 and SUMO2. $^{1}H-^{1}H$ TOCSY and $^{1}H-^{1}H$ NOESY experiments were acquired and used to assign SLS4. For NMR titration experiments, ~3 mM peptides were titrated into ~0.5 mM ^{15}N-SUMO1/2. The titration data were fit inthe protein:ligand (1:1) model using the equation $CSP_{obs} = CSP_{max}$ {($[P]_t$+$[L]_t$ + K_d) - [($[P]_t$+ $[L]_t$ + K_d)^2- 4$[P]_t[L]_t$]$^{1/2}$}/2$[P]_t$, where $[P]_t$ and $[L]_t$ are total concentrations of protein and ligand at any titration point. Intermolecular NOEs between SUMO1 and SLS4 were obtained by acquiring a ^{15}N-edited NOESY-HSQC on a ^{2}H, ^{15}N-SUMO1/SLS4 (1:5) complex sample with a mixing time of 300 ms. A reference ^{15}N-edited NOESY-HSQC of free SUMO1 was used to rule out any intramolecular NOEs arising from incomplete deuteration of SUMO1. Intermolecular NOEs between SUMO2 and SLS4 were measured similarly. ^{13}C, ^{15}N-filtered (F1), ^{13}C, ^{15}N-edited (F2) NOESY HSQC was collected on a ^{13}C, ^{15}N-SUMO1/ppSLS4 (1:1.5) complex sample with a mixing time of 200 ms to measure intermolecular NOEs between SUMO1 and ppSLS4. A similar experiment was performed to obtain intermolecular NOEs in the SUMO2/ppSLS4 complex. The Chk2-FHA domain was assigned by standard HNCO, HN(CA)CO, HNCA, and HN(CO)CA experiments on a 180 μM $^{13}C-^{15}N$-FHA-Chk2 sample. For NMR titration experiments, 2.4 mM ICP0-FBM was titrated into 65 μM ^{15}N-labeled Chk2-FHA domain.

Structural studies

Unambiguous restraints between the SUMO1 and SLS4 were determined from the intermolecular observed NOEs. The assignments of SLS4 resonances were carried out by 2D $^{1}H-^{1}H$ TOCSY and $^{1}H-^{1}H$ NOESY experiments. The structural model of SLS4 was determined using torsion angles from $^{1}H\alpha$ assignments and $^{1}H-^{1}H$ NOESY restraints in xplor-NIH. The structural model of the SUMO1/SLS4 complex was calculated in HADDOCK [23] using the structure of SUMO1 (PDB ID: 4WJO) and the extended structural model of SLS4. Rigid body energy minimization generated one thousand initial complex structures, and the best 200 lowest energy structures were selected for torsion angle dynamics and subsequent Cartesian dynamics in an explicit water solvent. Default scaling for energy terms was applied. The interface of SUMO1 was kept semiflexible during simulated annealing and the water refinement steps. Following the standard benchmarked protocol, cluster analysis of the 200 water refined structures yielded a single ensemble. The SUMO2/SLS4 complex was similarly docked, except that intermolecular restraints between SUMO2 and SLS4 were used and the starting structure of SUMO2 was taken from a crystal structure of free SUMO2 (PDB ID: 1WM3). The SUMO1/ppSLS4 and SUMO2/ppSLS4 complexes were docked using intermolecular NOEs obtained from the ^{13}C, ^{15}N-filtered (F1), ^{13}C, ^{15}N-edited (F2) NOESY HSQC experiments. An extended structural model of FBM peptide was obtained in a manner similar to SLS4. We determined the Chk2-FHA/FBM model by docking the Chk2-FHA (PDB ID: 1GXC) and the FBM peptide using CSPs observed in the NMR titration experiments.

In vitro assays

The *in vitro* polyubiquitination assays were performed using Ube1 (0.5 μM), Ube2d1 (3 μM), E3s ICP0-R, ICP0-RS4 and its mutants (5 μM), and 50 μM Ub. The reaction mixture was incubated at 37 °C for 45 min in the reaction buffer containing 50 mM Tris (pH 7.5), 50 mM NaCl, 2 mM $MgCl_2$, and 5 mM ATP. The reaction was quenched with 5 mM EDTA and 4xSDS gel loading buffer and resolved on 12% Bis-Tris gel. The gel was transferred onto polyvinylidene difluoride (PVDF) and blotted with anti-Ub antibody (ENZO-P4D1) as per the manufacturer's protocol. The chemiluminescence was observed by clarity Enhanced Chemi Luminescence (Bio-Rad) staining in Image Quant LAS 4000 (GE). The SUMO2 chains were used as a substrate (100 ng) and blotted with the anti-SUMO2 antibody to observe the ubiquitination of SUMO2 chains. In another set of reactions, the ubiquitination was carried out on SUMO capture affinity beads (Enzo), quenched and washed (3×) with high salt buffer, followed by blotting using an anti-Ub monoclonal antibody. For the assay with a phosphomimetic mutant of ICP0-RS4, the concentration of ICP0-RS4 and ICP0-RS4pm was 0.5 μM, and the reaction time was 20 min. The STUbL assays with full-length ICP0 (or its mutants) with SUMO2 chains were performed by incubating Ube1 (1 μM), Ube2d1 (5 μM), ICP0 or its mutants (10 μM), Alexa Fluor Maleimide (Invitrogen) labeled Ub (20 μM) with SUMO2 chains on SUMO capture beads for 30 min at 37 °C, quenched and washed (3×), and separated on a 12% Bis-Tris SDS gel and visualized in Uvitec (Cambridge). For the STUbL assays with FLAG-PMLs or FLAG-Sp100s, a SUMOylation reaction was first carried out with SAE1/2 (4 μM), Ubc9 (30 μM), SUMO2 (150 μM), and FLAG-PMLs or FLAG-Sp100s (150 μM) at 37 °C. The reaction was subsequently incubated on anti-FLAG affinity beads (Sigma) and washed (3×), and the ubiquitination assay was carried

out on the beads similar to that for SUMO2 chains. The STUbL assays with GST-PML were performed similarly, except the reaction was incubated on Protino Glutathione Agarose (Thermo Scientific). For the kinetic analysis with ICP0 and ICP0pm, the enzyme concentrations were Ube1 (1 μM), Ube2d1 (2 μM), ICP0 or ICP0pm (2 μM), and SUMO2 chains (0–3 μM). The deSUMOylation reactions were carried out by treating with 5 μM SENP2 for 2–3 h.

For the phosphorylation assays, 10 μg ICP0–S was incubated with 0.5 μg Chk2 (Origene) for 30 min at 30 °C in a 20 μl reaction containing 50 mM Tris (pH 7.5), 10 mM $MgCl_2$, 10 mM $MnCl_2$, 5 mM DTT, and 5 mM ATP. The entire phosphorylation reaction was directly digested with trypsin and used for mass spectrometry. Phosphorylation assays of ICP0 with CK1 and Chk2 were performed by incubating 20 μg his_6-ICP0 with 0.5 μg CK1δ (Merck Millipore) and 0.5 μg ChK2 (Origene) in buffer containing 50 mM Tris (pH 7.5), 10 mM $MgCl_2$, 10 mM $MnCl_2$, 5 mM DTT, and 5 mM ATP on Ni^{2+} NTA-agarose beads (Protino). Subsequent to the kinase reaction, beads were washed (3×) and ICP0 was eluted by 200 mM imidazole, dialyzed, and used for STUbL assays. CK1 inhibition was carried out by using PF5006739 (Sigma) at 0.2 mM concentration. ChK2 inhibition was carried out by using 2-(4-(4-Chlorophenoxy) phenyl)-1H-benzimidazole-5-carboxamide hydrate (Sigma) at 0.2 mM concentration.

Cell culture and transfection

HEK293T cells were maintained in DMEM with 10% serum. One 100 mm dish was transfected with 10 μg GFP-ICP0 plasmid with Lipofectamine 3000. Immunoprecipitation (IP) was performed by 36-h post-transfection. Anti-GFP sepharose beads (Cell Signaling Technology) were used for IP, according to the protocol provided by the manufacturer. After IP, beads were directly loaded onto reducing SDS PAGE to resolve immunoprecipitated proteins. The band, matching the size of the protein of interest, was excised and analyzed by mass spectrometry.

Mass-spectrometry

Samples were digested in the National Centre for Biological Sciences proteomics facility using an established protocol [57]. For LC-LTQ Orbitrap MS analysis, samples were resolubilized in 2% [v/v] acetonitrile, 0.1% [v/v] formic acid in water and injected onto an Agilent1200 (Agilent, Santa Clara, CA, USA) nanoflow LC system that was in-line coupled to the nanoelectrospray source of a LTQ-Orbitrap Discovery hybrid mass spectrometer (Thermo Scientific, SanJose, CA, USA). Peptides were separated on Zorbax 300SB-C18 (Agilent, Santa Clara, CA, USA) by a gradient developed from 2% [v/v] acetonitrile, 0.1% [v/v] formic acid to 80% [v/v] acetonitrile, and 0.1% [v/v] formic acid in water over 70 min at a flow rate of 300 ml/min. Full MS in a mass range between *m/z* 300 and *m/z* 2000 was performed on an Orbitrap mass analyzer with a solution of 30,000 at m/z 400 and an AGC target of 2×10^5. The strongest five signals were selected for CID-MS/MS in the LTQ ion trap at a normalized collision energy of 35% using an AGC target of 1×10^5 and two micro scans. Dynamic exclusion was enabled with one repeat counts during the 45s and an exclusion period of 120s. Peptide identification was performed by CID-based MS/MS of the selected precursors, which also revealed the site of phosphorylation modification. For protein-peptide identification, MS/MS data were searched against the custom peptide sequence provided by LifeTein using PEAKS Studio X software. The search was set up for full tryptic peptides with a maximum of three missed cleavage sites. Oxidized methionine, serine, and threonine were included as variable modifications. The precursor mass tolerance threshold was 10 ppm, and the maximum fragment mass error was 0.5 Da. The peptide identification was made at 1% False Discovery Rate.

The proteomics of full-length ICP0 was performed at VProteomics (http://www.vproteomics.com/). The ICP0 gel band was excised, reduced with 5 mM TCEP, alkylated with 50 mM iodoacetamide, and then digested with trypsin (1:50, trypsin/lysate ratio) for 16 h at 37 °C. Digests were cleaned using a C18 silica cartridge to remove the salt and dried using a speed vac. The dried pellet was resuspended in buffer A (5% acetonitrile, 0.1% formic acid). All the experiments were performed using EASY-nLC 1000 system (Thermo Fisher Scientific) coupled to Thermo Fisher-QExactive equipped with nanoelectrospray ion source.One microgram of the peptide mixture was resolved using 25 cm a PicoFrit column (360 μm outer diameter, 75 μm inner diameter, 10 μm tip) filled with 1.9 μm of C18-resin (Dr. Maeisch, Germany). The peptides were loaded with buffer A and eluted with a 0–40% gradient of buffer B (95% acetonitrile, 0.1% formic acid) at a flow rate of 300 nl/min for 45 min. MS data were acquired using a data-dependent top10 method dynamically choosing the most abundant precursor ions from the survey scan.

In data processing, RAW files generated were analyzed with Proteome Discoverer (v2.2) against the proteome database. For the sequest search, the precursor and fragment mass tolerances were set at 10 ppm and 0.5 Da, respectively. The protease used to generate peptides, that is, enzyme specificity, was set for trypsin/P (cleavage at the C terminus of "K/R: unless followed by "P") along with maximum missed cleavages value of two. Carbamidomethyl on cysteine as fixed modification and oxidation of methionine and N-terminal acetylation and phospho (S, T, and Y) were considered as variable modifications for database search. Both peptide spectrum match and protein false discovery rate were set to 1% FDR.

The quantification of phosphorylation was performed by parallel reaction monitoring (PRM) analyses performed using the Q-Exactive mass spectrometer (Thermo Scientific, Bremen, Germany). Analysis of single peptide was performed on a Q-Exactive instrument. The acquisition method had a scheduled PRM from the 20–35 min RT event. The PRM event was performed with an Orbitrap resolution of 17,500 (at *m/z* 200), a target AGC value of 1e6, and maximum fill times of 100 Ms. Fragmentation was acquired with a normalized collision energy of 27 eV, and MS/MS scan range of *m/z* 100–1500 was used for mass determination. All the PRM data analysis were performed using skyline-Daily software, version 19.1.0.193 (https://skyline.ms/project/home/begin.view).

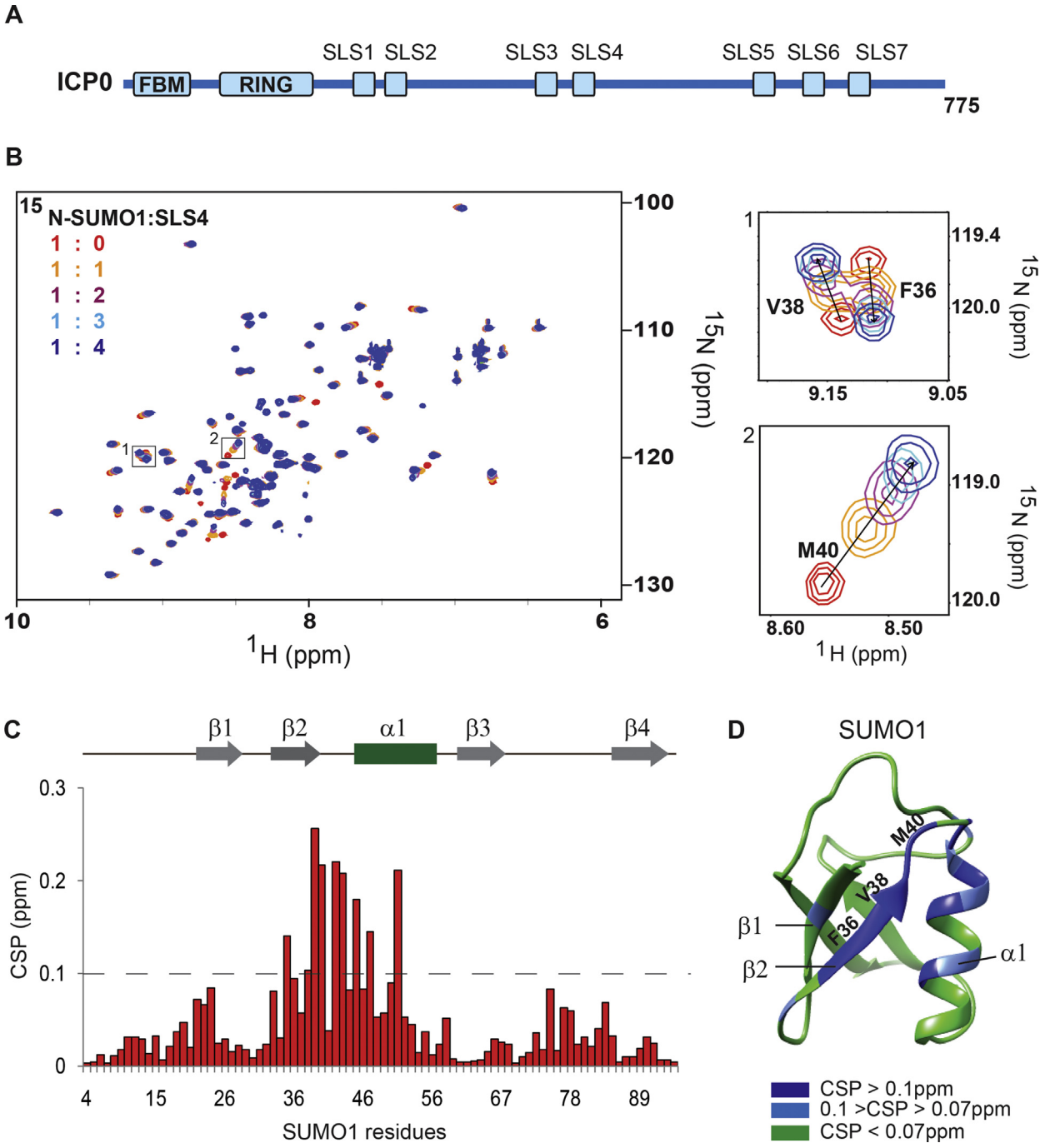

Fig. 1. Interactions between SLS4 and SUMO1 studied by NMR. (A) The domains in ICP0 relevant to this study. The FHA binding motif (FBM), the RING finger domain, and the SLS domains are shown. (B) Overlay of the ^{15}N-edited HSQC spectra of free SUMO1 (red) with different stoichiometric ratios of SLS4 as given in the top left-hand side of the spectra. Two regions of the spectra are expanded to show SUMO1 peak shifts upon titration with SLS4. The chemical shift perturbations (CSP) between the free and the bound form are calculated as CSP $= [(\delta^{H}_{free} - \delta^{H}_{bound})^2 + ((\delta^{N}_{free} - \delta^{N}_{bound})/5)^2]^{1/2}$, where δ^{H} and δ^{N} are the chemical shift of the amide hydrogen and nitrogen, respectively. (C) The CSPs for each residue in SUMO1 upon binding to SLS4. The black dashed line indicates a 2*standard deviation. The residues with CSPs significantly above the dashed line are probably at the interface of the SUMO1-SLS4 complex. The secondary structure alignment of SUMO1 against its sequence is provided above the plot. (D) Significant CSPs mapped on the SUMO1 structure. The residues corresponding to the expanded spectra in (B) are labeled on the structure. SUMO, small ubiquitin-like modifier; SLS, SIM-like sequence; SIM, SUMO-interacting motif; HSQC, heteronuclear single quantum coherence; NMR, Nuclear Magnetic Resonance.

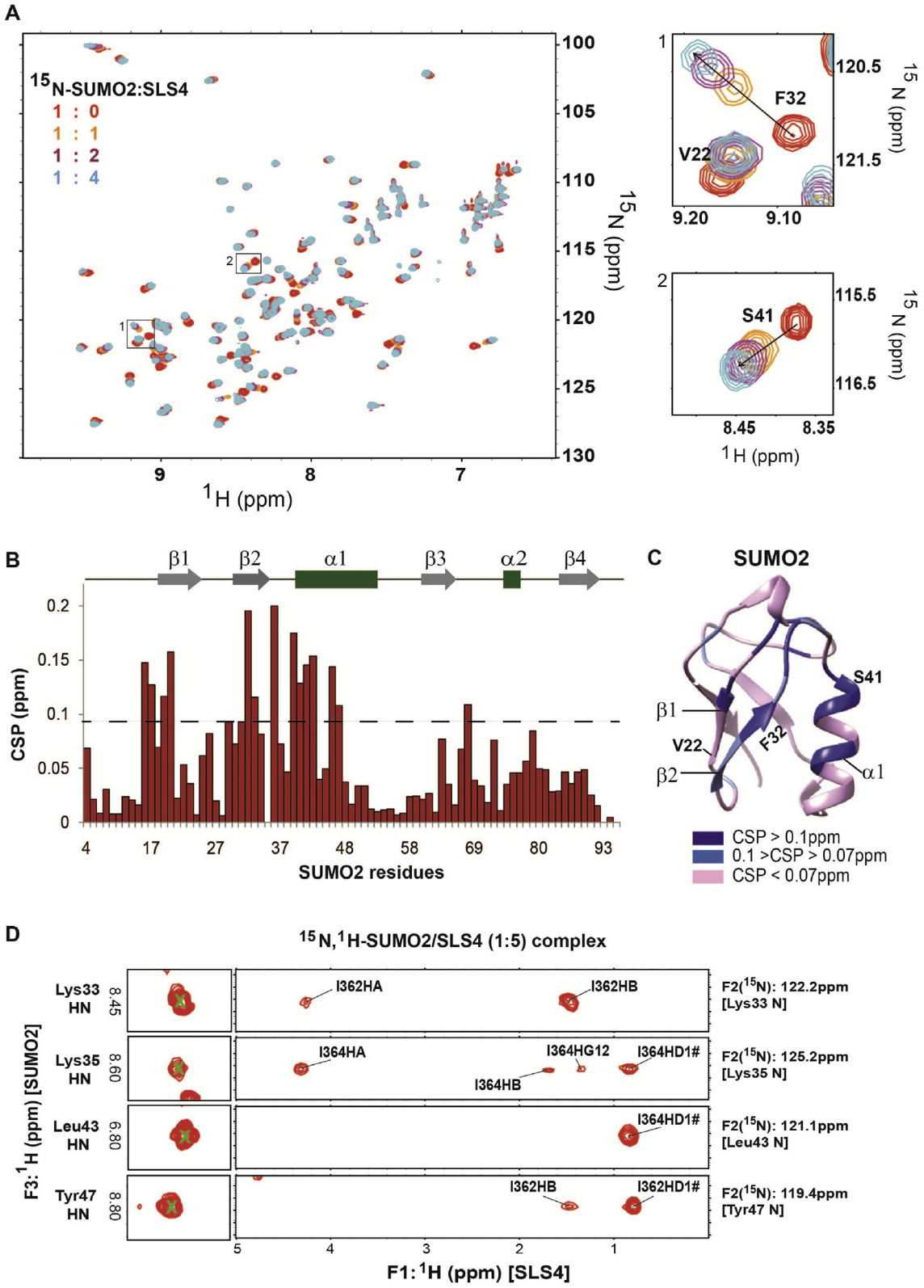

Fig. 2. Interactions between SLS4 and SUMO2 studied by NMR. (A) Overlay of the ^{15}N-edited HSQC spectra of free SUMO2 (red) with different stoichiometric ratios of SLS4 as given in the top left-hand side of the spectra. Two regions of the spectra are expanded to show SLS4 induced shifts in the SUMO2. The chemical shift perturbations (CSP) between the free and the bound form are calculated as given in Fig. 1 legend. (B) The CSPs observed in SUMO2 upon binding SLS4

Viral growth and plaque assay

The Vero cell line was purchased from the NCCS, Pune Cell Repository and was grown at 37 °C and 5% CO2 in Dulbecco's modified Eagle's medium (DMEM) supplemented with 10% Fetal Bovine Serum, 100 U/ml of penicillin, and 100 μg/ml of streptomycin. The wt-HSV1 17 syn + strain was a kind gift from Karen L Mossman, which was propagated and tittered in the Vero cell line [58]. Vero cells were grown in a 60 mm tissue culture dish. Before infection, the cells were pretreated with CHK2 inhibitor (10 μM) for 1 h. Control cells were treated with DMSO. Infection was carried out using wt-HSV1 17 syn + strain at MOI of 0.1 for 2 h at 37 °C. After 2 h viral inoculum was removed and fresh medium was added with inhibitor. Cells and the medium were harvested at various time point after infection (12, 24, 36, 48 and 60 h), then lysed by freeze and thaw cycles. Serial 10-fold dilutions of the lysate were prepared. Each dilution was used to infect the monolayers of Vero cell lines in triplicate. Infection was carried out for 2 h at 37 °C with intermittent rocking. After infection, the viral inoculum was removed and the fresh DMEM medium containing 1% heat-inactivated serum and 0.5% methylcellulose was added. After three days of incubation at 37 °C, cells were washed with PBS and fixed with methanol for 15 min at room temperature followed by staining with 1X Giemsa stain. The plaques were counted and imaged using a 4× objective in a fluorescence microscope. The proteomics data are submitted at Proteomics Identification Database with accession number PXD014671.

MD simulations

All-atom MD simulations of SUMO1/ppSLS4 and SUMO2/ppSLS4 were run on GPU clusters using NAMD [59]. The protein and ions were described with the CHARMM36 force field [60,61] and water molecules with the TIP3P model. The proteins were solvated in a water box extending 12 Å from the outermost protein atom. The simulations were started from experimentally determined NMR structures and were energy minimized. The energy-minimized structures were allowed to equilibrate for 5 ns before the production run started. A time step of 2fs was used with the bonds involving hydrogen atoms being constrained using the SHAKE algorithm [62,63]. Electrostatic interactions were calculated using the Particle mesh Ewald method [64], and the van der Waals interactions were truncated beyond 12 Å. Periodic boundary conditions were imposed in all directions. The temperature of the systems was controlled at 300 K using the Langevin dynamics, and the pressure was kept at 1 atm using the Nose-Hoover Langevin piston method [65,66]. The data were analyzed and plotted using VMD [67], UCSF-Chimera [68], and Matlab.

Isothermal titration calorimetry

The purified FHA-Chk2 and the synthetic peptide of ICP0-FBM were dissolved in buffer (50 mM phosphate, 300 mM NaCl [pH 7.4]). The 750 μM peptide solution was injected into a sample cell containing 50 μM FHA-Chk2 at 25^{O}C. The measurement was performed on a Microcal ITC_{200} (GE Healthcare), and binding isotherm was plotted and analyzed using Origin (v7.0). Integrated interaction heat values from individual experiments were normalized, and the data were fit, omitting the first point, using a single binding site model.

Results

SLS4 is the sole bona fide SIM in ICP0

One or more of the seven predicted SLS domains in ICP0 (SLS1-SLS7)[16] could be responsible for targeting SUMOylated substrates (Fig. 1A). Hence, all seven domains were tested for binding to the SUMO. Seven peptides were designed corresponding to the SLS domains (Table S1). The affinity of the SIM domains for SUMOs is typically weak [17]. Because NMR spectroscopy can detect binding over a broad range of affinities, including very weak affinities, the binding of SLS domains to SUMO1 and SUMO2 was tested by NMR. SLS4 was titrated into a sample of ^{15}N isotope-labeled SUMO1, and the effect on SUMO1 was detected by ^{15}N-edited heteronuclear single quantum coherence (HSQC) experiments. Perturbations due to the altered chemical environment upon ligand binding induce changes in the chemical shift of the backbone amide resonances (Fig. 1B). The chemical shift perturbations (CSPs) plotted in Fig. 1C show that the maximal perturbations upon binding SLS4 occur in the region between β2 and α1 of SUMO1 (Fig. 1D), which was identified as the binding site of SLS4. SIMs from PML, RNF4, and PIASX bind to a similar region in the SUMO [17,20,21]. The same titration experiments were repeated for other SLS domains. However, none of the other SLS domains showed any consistent peak shifts in the SUMO1 spectra upon titration (an example titration of SLS7 is given in Fig. S1A), indicating that the other SLS domains do not bind SUMO1. The shifts in amide resonances in the SUMO1/SLS4 titration spectra was fit against the ligand:protein concentration ratio to yield the K_d of 128 (±13) μM (Fig. S2A).

are shown. The dashed line shows the 2*standard deviation. (C) Significant CSPs mapped on the SUMO2 structure. The residues corresponding to the expanded spectra in (A) are labeled on the structure. (D) Selected strips from the ^{15}N-edited NOESY-HSQC spectra depicting intermolecular NOEs between amide protons of SUMO2 and protons of the SLS4 domain. ^{15}N and ^{1}H assignment of SUMO2 amide atoms are given on the right and left of the strips, respectively. The protons of SLS4 that show NOEs to SLS4 are assigned. SUMO, small ubiquitin-like modifier; SLS, SIM-like sequence; SIM, SUMO-interacting motif; HSQC, heteronuclear single quantum coherence; NMR, Nuclear Magnetic Resonance.

The titration experiments were repeated with ^{15}N-labeled SUMO2 and SLS4 and monitored using the ^{15}N-edited HSQC spectra of SUMO2 (Fig. 2A). Apart from a few long-range CSPs in β1 beta-strand of SUMO2, most CSPs occurred in the region between β2 and α1 (Fig. 2B and C). None of the other SLS domains induced consistent shifts in the SUMO2 amide resonances upon titration (Fig. S1B). The shifts in amide resonances in the SUMO2/SLS4 titration spectra were fit against the ligand:protein concentration ratio to yield K_d of 81 (±17) μM (Fig. S2B). It has been indicated recently that the region, including the SLS domains SLS5, SLS6, and SLS7, could be important for binding SUMOs [16]. Hence, SUMO1 and SUMO2 were titrated against a peptide that included SLS5, SLS6, and SLS7 (SLS567). However, SLS567 did not bind SUMO2 (Figs. S3A and S3B) and interacted very weakly with SUMO1 (Fig. S3C). Because SLS4 is the only SLS domain in ICP0 that binds SUMO1 or SUMO2, it was identified as the sole bona fide SIM in ICP0.

Structural analysis of the SUMO1/SLS4 and the SUMO2/SLS4 complexes

The structural model of SUMO1/SLS4 and SUMO2/SLS4 complexes was determined to obtain molecular details of their interaction. Two=dimensional (2D) ^{1}H−^{1}H TOCSY and ^{1}H−^{1}H NOESY experiments provided the proton chemical shifts of SLS4. Although the SLS4 peptide used in the experiments was twenty amino acids long, only the central twelve amino acids (N357−P368) exhibited resonances in the amide region in the ^{1}H−^{1}H TOCSY and ^{1}H−^{1}H NOESY spectra of the peptide, indicating that the N- and C-terminal regions of SLS4 are dynamic, and their resonances are broadened because of conformational exchange. ^{15}N-edited NOESY-HSQC experiment was carried out on a ^{15}N, ^{2}H-labeled-SUMO2/SLS4 (1:5) complex to obtain intermolecular NOEs between SUMO2 and SLS4 (Fig. 2D). The ^{1}Hα values in SLS4 were compared with the random chemical shift values, which indicated that SLS4 had the propensity to form beta-strand (Fig. S4A)[22]. The HN-Hα NOE also confirmed that SLS4 has the propensity to form beta-strand (Fig. S4B). Hence, the model of SLS4 was determined using beta-strand torsion angles and the ^{1}H−^{1}H NOESY restraints. Using the SLS4 structure, SUMO2 structure (PDB: 1WM3), and the intermolecular NOEs as distance restraints, the structural model of the SUMO2/SLS4 complex was determined by HADDOCK [23]. The refinement statistics are provided in Table 1. Fig. S5A shows the twenty lowest energy structures, which superimposed with a root-mean-square deviation (rmsd) of 0.6 Å. The lowest energy model given in Fig. 3A verified that SLS4 binds to the region between β2 and α1 as predicted by CSPs from the titration experiment. SLS4 forms a β-strand parallel to the β2 strands of SUMO2.

Both the hydrophobic and electrostatic interactions contribute to the binding between SUMO2 and SLS4. A set of hydrophobic contacts are observed between the central SLS4 residues (PIVI) and the β2-strand of SUMO2 (Fig. 3A, Fig. S5B, Table S2). A hydrophobic shallow groove is present between β2 and α1 in SUMO2, and the hydrophobic side chains of the SLS4 reciprocate this groove (Fig. 3C). SUMO2 has a significant positively charged surface at the SIM binding interface (Fig. 3C), which complements the negatively charged residues in SLS4. Hence, a network of salt bridges forms at the N- and C-termini of the central SLS4 region, which stabilizes the SUMO2/SLS4 interaction (Fig. 3A).

^{15}N-edited NOESY-HSQC on a sample of ^{15}N, ^{2}H-SUMO1/SLS4 (1:5) complex detected the intermolecular NOEs between SUMO1 and SLS4 (Fig. S6A). The structural model of the SUMO1/SLS4 complex was determined using the measured intermolecular NOEs (Table 1). The twenty lowest energy structures superposed with an rmsd of 0.7 Å (Fig. S6B). The lowest energy model given in Fig. 3B shows that SLS4 binds to the region between β2 and α1 in SUMO1 as predicted by the CSPs. The packing of hydrophobic surfaces and the surface charge complementation were also evident in the SUMO1/SLS4 complex (Fig. 3D and S5C, Table S3).

The SLS4 and the RING finger domain is sufficient for STUbL activity of ICP0

STUbLs include two essential domains, the RING finger domain that interacts with the E2~Ub conjugate and SIM domains that interact with the SUMOylated substrates [14,24]. ICP0 includes both the catalytic RING finger and the bona fide SIM SLS4. Two chimeras were prepared to investigate if these two domains in ICP0 are sufficient for its STUbL activity: ICP0-R and ICP0-RS4. ICP0-R includes the RING finger domain of ICP0, and ICP0-RS4 includes both the RING finger domain and the SLS4 domain (Fig. 3E). A ubiquitination reaction with Ube1 (E1), Ube2d1 (E2), Ub, and either ICP0-R or ICP0-RS4 was carried out at 37 °C. Both the chimeras could catalyze polyubiquitin chains owing to the presence of the RING finger domain (Fig. S7A). Then the STUbL activity of these chimeras was examined by their ability to ubiquitinate SUMO2 chains (as a substitute of the SUMOylated substrate). The ubiquitination reaction was repeated in the presence of SUMO2 chains. ICP0-RS4 could identify SUMO2 chains and assemble polyubiquitin chains on them, whereas ICP0-R could not (Fig. 3G and H). When the central hydrophobic Ile362-Val363-Ile364 residues in SLS4 were mutated to alanines, the ubiquitination activity of

Table 1. NMR and refinement statistics of the SUMO/SLS4 complexes.

NMR restraints and structural statistics	SUMO1/SLS4	SUMO2/SLS4
Unambiguous restraints (NOE)	14	18
Dihedral restraints (phi,psi)	24	24
HADDOCK parameters		
Cluster size	200	200
HADDOCK score	−84.1 (±4.8)	−68.5 (±0.5)
Van der Waals energy	−42.4 (±5.7)	−35.0 (±2.9)
Electrostatic snergy	−275.1 (±22.3)	−271.0 (±7.3)
Restraints violation energy	+1.2 (±0.66)	+2.8 (±0.9)
Buried surface area	+1232.5 (±32.6)	+1226.9 (±49.0)
Rmsd[a] (Å)		
All backbone	0.5	0.3
All heavy atoms	0.7	0.6
Molprobity[b]		
Clash score	4.2	3.5
Score	2.5	2.3
Ramachandran plot[b]		
Most Favored regions	88.2	85.3
Allowed regions	8.8	13.2
Generous regions	1.5	0.0
Disallowed regions	1.5	1.5

SUMO, small ubiquitin-like modifier; SLS, SIM-like sequence; SIM, SUMO-interacting motif; NMR, Nuclear Magnetic Resonance.
[a] Calculated for an ensemble of 20 lowest energy structures.
[b] Calculated for the lowest energy structure.

ICP0-RS4 was unaffected, but its STUbL activity diminished (Fig. 3H and Fig. S7B). A similar effect was observed when the negatively charged residues flanking the central region Asp360 and Asp366 were mutated to positive charges (Fig. 3H). When the experiments were repeated with full-length ICP0 and its mutants (Fig. 3F and Fig. S7D), the results were similar (Fig. 3I), indicating that the mechanism of STUbL activity is similar between the full-length ICP0 and the ICP0-RS4 chimera. Altogether, these results demonstrate that the RING domain and SLS4 are necessary and sufficient for the STUbL activity of ICP0. Moreover, both the electrostatic and hydrophobic interactions between SUMO and SLS4 are significant for STUbL activity.

ICP0 ubiquitinates both the substrate and SUMO in the poly-SUMOylated substrate

Although ICP0 can identify and ubiquitinate free $(SUMO)_n$ chains in solution, further experiments were carried out to assess if it can identify and ubiquitinate SUMOylated substrates. Three substrates were used to test the function of ICP0 (Fig. 4A). The first substrate was a short region of PML (PMLs, amino acids:485−495), which includes the consensus SUMOylation site in PML K490 [25]. The second substrate was a short region of PML NB constituent protein Sp100 (Sp100s, aa:292−305), which includes its consensus SUMOylation site K297 [26]. The third substrate is a long stretch of amino acids in the N-terminal region of PML (PML, aa:370−570), which includes the consensus SUMOylation site K490 and multiple ubiquitination sites as predicted by UbPred and UbiSite [27,28]. A SUMOylation reaction with either FLAG-PML or FLAG-Sp100 confirmed that they are indeed SUMOylated *in vitro* (Fig. 4B). The SUMOylation reaction was captured on anti-FLAG affinity beads and washed to get rid of SUMOylation enzymes and free SUMO2 (Fig. S7E). Then an ubiquitination reaction was carried out on the beads using Ube1, Ube2d1, ICP0, and Alexa-Ub. After the reaction, Ethylenediaminetetraacetic acid (EDTA) was used to quench the reaction; the beads were washed thoroughly to get rid of the ubiquitination enzymes and any free polyubiquitin chains in solution. After washing, the beads containing ubiquitinated-SUMOylated substrate ($(Ub)_n$~$(SUMO)_n$~FLAG-PMLs) were detected. Although ICP0 could identify and ubiquitinate SUMOylated FLAG-PMLs, the mutants ICP0m1 and ICP0m2 could not, validating that the electrostatic and hydrophobic interactions at the SUMO/SLS4 interface are critical for the STUbL activity (Fig. 4C). Similarly, SUMOylated FLAG-Sp100s was ubiquitinated by ICP0 but not by ICP0m1 or ICP0m2 (Fig. 4D).

Much similar to the shorter region of PML, the more extended region of PML fused to an N-terminal Glutathione S-transferase (GST) tag was SUMOylated *in vitro* (Fig. 4E). The SUMOylation was not on the N-terminal GST (Fig. S7F). The SUMOylation reaction was captured on Glutathione Agarose beads and washed to get rid of SUMOylation enzymes and free SUMO. Consequently, ubiquitination reaction was carried out using Ube1, Ube2d1,

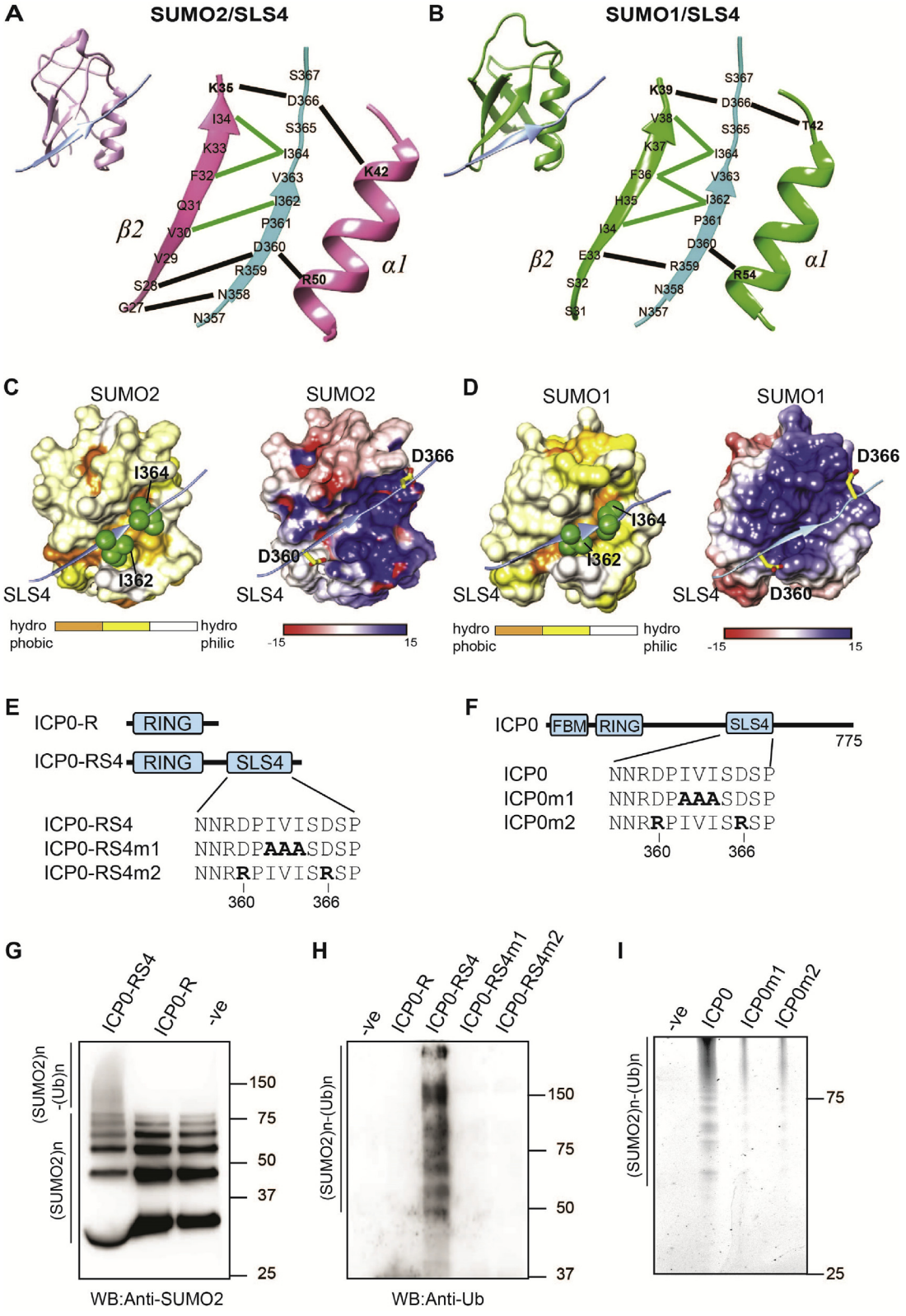

Fig. 3. The hydrophobic and electrostatic contacts at the SUMO/SLS4 complex are essential for the STUbL activity of ICP0. Left-hand corner in (A) and (B) represents the lowest energy structure of the SUMO2/SLS4 and SUMO1/SLS4 complex, respectively. SUMO2 is colored in pink, SUMO1 is colored in green, and SLS4 is colored in light blue. The interface between SLS4 and SUMO1/2 is expanded on the right. The salt bridges between SLS4 and SUMO1/2 are shown

ICP0, and Alexa-Ub, washed, and the beads were separated on SDS gel for visualization. ICP0m1 and ICP0m2 could not ubiquitinate SUMOylated PML as efficiently as ICP0 (Fig. 4F). If the SUMOylated PML was cleaved by deSUMOylating enzyme SENP2 and washed before ubiquitination, ICP0 could not ubiquitinate PML effectively, indicating that ICP0 specifically targets SUMOylated PML (Fig. 4G). Another experiment was carried out to detect if ICP0 assembles polyubiquitin chains directly on the substrate PML or on the poly-SUMO chains conjugated to PML (Fig. 4H). After the ubiquitination reaction, the beads were washed, treated with SENP2, and then spun to separate the GST-PML and SUMO chains, followed by detection. ICP0 ubiquitinates both the PML and SUMO (Fig. 4I), suggesting a mechanism where the viral STUbL ensures that the substrate is marked for degradation and cannot be rescued by host deSUMOylating enzymes.

Phosphorylated SLS4 binds SUMO1 and SUMO2 with higher affinity

Phosphorylation of ICP0 can significantly regulate its activity [29–31]. Interestingly, a variant of ICP0 that cannot be phosphorylated at Ser365, Ser367, and Ser371 lacks the potency to degrade PML NBs [30]. When the phosphorylation of ICP0 was checked in HEK293T cells, Ser365, Ser367, and Ser371 were indeed phosphorylated (Fig. 5A). In the SUMO/SLS4 complex, Ser371 is dynamic and far from the SUMO/SLS4 interface. On the other hand, both Ser365 and Ser367 are present at the SUMO/SLS4 interface. The effect of phosphorylation at 365 on SUMO/SLS4 interaction was tested by using a pSLS4 peptide, which is similar to SLS4 but phosphorylated at Ser365 (Fig. 5B). These NMR titrations were carried out in conditions similar to the SLS4 titration. Fig. S8A shows the pattern of CSPs observed in SUMO2, which is similar to CSPs observed during the titration with SLS4, implying that the interface of pSLS4 is similar to SLS4. However, the magnitude of average CSP was higher, indicating that a higher population of the SUMO2/pSLS4 was in bound conformation compared with SUMO2/SLS4 at the same protein to ligand ratio and implying that pSLS4 has a higher affinity for SUMO2 than SLS4. Indeed, upon fitting the titration data, K_d was found to be 7 (±2) μM for pSLS4 compared with the 81 (±17) μM for SLS4 (Fig. 5C, Fig. S8B).

The titration was repeated with diphosphorylated SLS4 (ppSLS4), where both Ser365 and Ser367 are phosphorylated (Fig. 5B). The pattern of CSPs was similar, except for a slight increase in the average magnitude compared with pSLS4 (Fig. 5D). A few peaks showed the pattern of intermediate exchange due to the increase in affinity (Fig. 5E). The K_d was determined by fitting peak shifts for the resonances that have less CSP and are still in fast exchange. The K_d was determined to be 3 (±1) μM (Fig. 5C, Fig. S10A).

When pSLS4 was titrated to SUMO1, the interface of pSLS4 was similar to SLS4 (Fig. S9A). However, the average CSP was higher when compared with SLS4. Fitting the titration data yielded the K_d of 16 (±5) μM (Fig. S9B). When titrated with the ppSLS4, the CSP pattern was conserved, but few peaks went into intermediate exchange (Fig. 5F and G). The peak shifts against SLS4 concentration were fit to yield the K_d of 5 (±2) μM (Fig. 5C, Fig. S10B). Altogether, phosphorylation increased the affinity of SLS4 for SUMO by ~25-fold.

The phosphorylated side chains of SLS4 make new electrostatic contacts with SUMOs

The structure of ppSLS4 in complex with SUMO2 and SUMO1 was determined to understand the mechanism of the phosphorylation induced increase in SUMO/SLS4 affinity. A ^{13}C, ^{15}N-filtered (F1), ^{13}C, ^{15}N-edited (F2) NOESY HSQC was acquired on a sample of ^{13}C, ^{15}N-SUMO2/ppSLS4 at the stoichiometric ratio of 1:1.5 (SUMO2:ppSLS4) (Fig. 5H). $^{1}H-^{1}H$ TOCSY and $^{1}H-^{1}H$ NOESY experiments provided the proton chemical shifts of ppSLS4. The chemical shifts of SUMO2 were assigned by

as black lines. The hydrophobic contacts between the central PIVI residues in SLS4 and SUMO1/2 are shown as green lines. (C) The surface representation of hydrophobic regions of SUMO2 in the SUMO2/SLS4 complex is shown on the left side. The surfaces are colored according to the hydrophobicity scale given in the following. The side chains of Ile362 and Ile364 in SLS4 are shown in green. The electrostatic surface of SUMO2 in the SUMO2/SLS4 complex is shown on the right side. Positive to negative charges are shown by blue to red. The Adaptive Poisson-Boltzmann Solver program calculated the electrostatic surface potential. The acidic residues of SLS4, Asp360, and Asp366 are shown in yellow. The side chain oxygen atoms are colored in red. (D) Same as (C) shown for SUMO1 in the SUMO1/SLS4 complex. (E) ICP0-R, ICP0-RS4, and its mutants used in this study. (F) ICP0 and its mutants used in this study. (G) Ubiquitination assays using Ube1 as E1, Ube2d1 as E2, and either ICP0-R or ICP0-RS4 as the E3, SUMO2 chains as the substrate and blotted with the anti-SUMO2 antibody. (H) A similar ubiquitination reaction as in (G) was carried out on SUMO2 affinity beads, and the beads were washed and blotted with the anti-Ub antibody. (I) Ubiquitination reaction similar to (H) using full-length ICP0 and E3 and Alexa-Ub as mutants of ICP0. The (-ve) control lane in (G), (H), and (I) lacks the E3. SUMO, small ubiquitin-like modifier; SLS, SIM-like sequence; SIM, SUMO-interacting motif; ICP0, infected cell polypeptide 0; STUbL, SUMO-targeted ubiquitin ligase; E3, ubiquitin ligase.

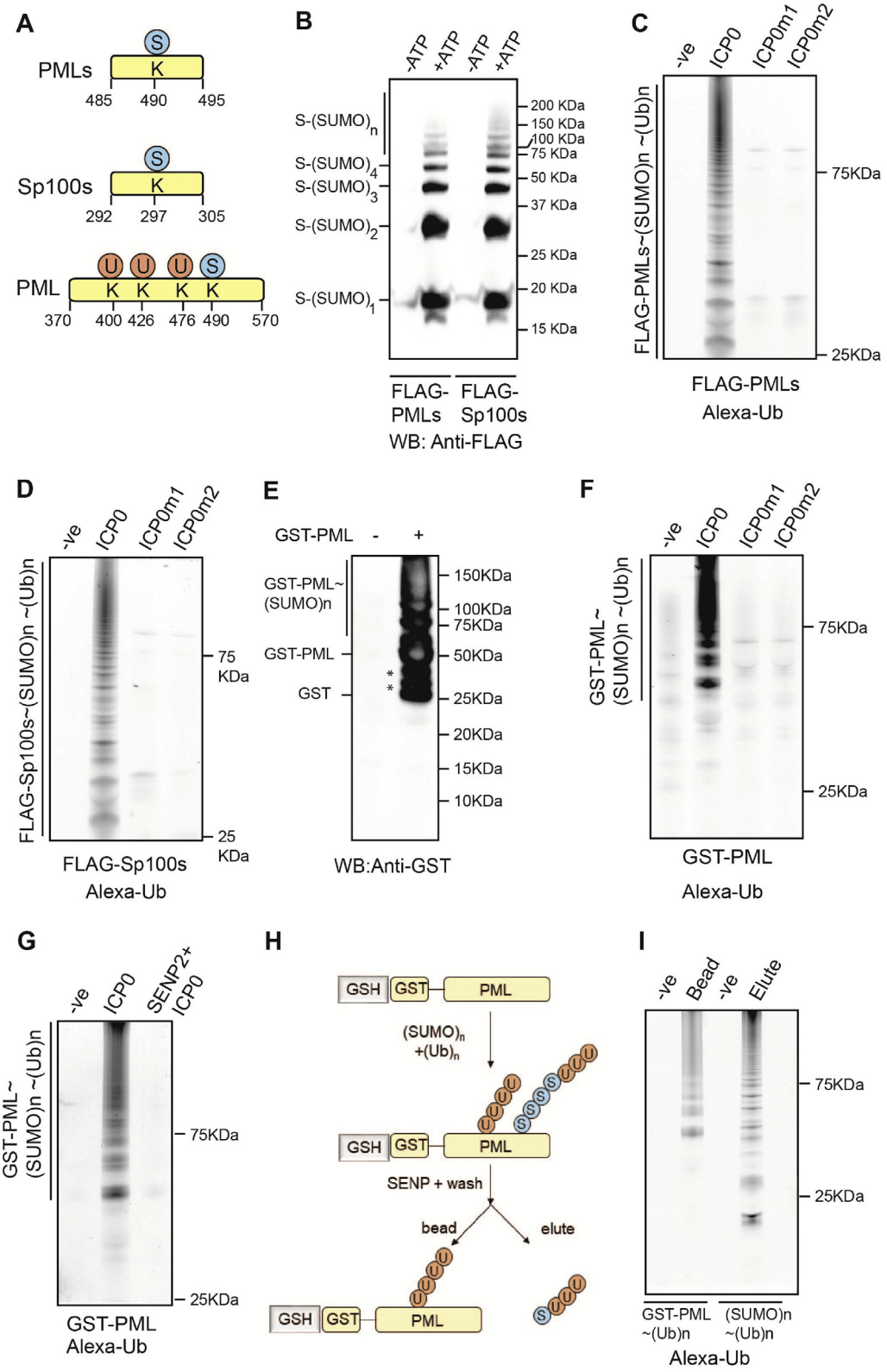

Fig. 4. Ubiquitination of SUMOylated substrates by ICP0. (A) Schematic of the substrates PMLs (aa: 485−490 of Promyelocytic leukemia protein (PML)), Sp100s (aa: 292−305 of protein Sp100), and PML (aa: 370−570 of protein PML). PMLs and Sp100s include the SUMOylation sites, while PML has both the SUMOylation site and predicted ubiquitination sites in PML protein. (B) SUMOylation of PMLs and Sp100s. SUMOylation reactions were carried out with FLAG-tagged

comparing the $^{15}N-^{1}H$ edited HSQC and $^{13}C-^{1}H$ edited HSQC of ^{13}C, ^{15}N-SUMO2/ppSLS4 complex with the assignments of apo SUMO2. Using the intermolecular NOEs as distance restraints, the structural model of the SUMO2/ppSLS4 complex was solved by HADDOCK [23] (Table 2 provides the structural statistics). Fig. S11A shows the twenty lowest energy structures, which superpose well with an rmsd of 0.7 Å. The model of SUMO2/ppSLS4 was overall similar to SUMO2/SLS4. Two new hydrogen bonds formed the phosphorylated SLS4 side chains and SUMO2 (Fig. 6A). Lysine 42 of α1 in SUMO2 now forms hydrogen bonds with the phosphate oxygen atoms of pSer365 and pSer367. These hydrogen bonds contribute to the increased affinity between SUMO2 and ppSLS4.

The structural model of the SUMO1/ppSLS4 complex was studied to determine if a similar mechanism operates between phosphorylated SLS4 and SUMO1. We prepared a sample of ^{13}C, ^{15}N-labeled SUMO1/ppSLS4 at the stoichiometric ratio of 1:1.5 (SUMO1:ppSLS4). ^{13}C, ^{15}N-filtered (F1), ^{13}C, ^{15}N-edited (F2) NOESY HSQC of this sample detected several intermolecular NOEs between SUMO1 and ppSLS4 (Fig. S11B), which were used to determine the SUMO1/ppSLS4 structural model. The twenty lowest energy models superimposed with a low rmsd of 0.6 Å (Fig. S11C). Three new hydrogen bonds were detected in the lowest energy model (Fig. 6B). The oxygen atom of phosphate groups of pSer365 and pSer367 form hydrogen bonds with lysine 46 present in α1. Phosphorylated Ser367 also forms a hydrogen bond with His43 of SUMO1.

Molecular dynamics (MD) simulations of the complexes between phosphorylated SLS4 and SUMO1/2 were carried out to estimate the stability of these new hydrogen bonds observed in the lowest energy structures. The complexes were dissolved in a square water box, equilibrated for 1ns, followed by NVT simulations. The phosphate oxygen atoms of Ser365 and Ser367 formed hydrogen bonds with the lysine 42 Nζ atom of SUMO2 practically throughout the simulation (Fig. 6C). The three oxygen atoms rotated about the central P=O double bond, but at any point in time, at least one of them was hydrogen bonded with lysine 42. Similarly, the hydrogen bond between Ser367 and lysine 42 Nζ was found to be reasonably stable (Fig. S12A). The hydrogen bonds between phosphoserines and SUMO1 were also stable throughout (Fig. 6D and Fig. S12B). Collectively, the structural studies and MD simulations reveal that phosphorylation creates new and stable hydrogen bonds between SUMO and SLS4, leading to the tighter binding of the SUMO/SLS4 complex.

Phosphorylation increases the STUbL activity of ICP0

The increased affinity between SLS4 and SUMO upon phosphorylation of SLS4 could increase the affinity of ICP0 for SUMOylated substrates. This was tested using a phosphomimetic mutant of ICP0-RS4. Ser365 and Ser367 were mutated to aspartic acids to create a phosphomimetic version of ICP0-RS4 (ICP0-RS4pm, Fig. 6E). The same phosphomimetic mutant was also made in the full-length ICP0 (Fig. 6E). The ubiquitination activity of ICP0-RS4pm is similar to ICP0-RS4, indicating that phosphorylation does not change the catalytic activity of the RING finger domain (Fig. S7C). Ubiquitination assay was carried out on poly-SUMO2 chains bound to the SUMO affinity capture beads, washed and blotted with the anti-Ub antibody. In the reaction, the concentration of E3 (ICP0-RS4 or ICP0-RS4pm) was reduced such that the E3:substrate stoichiometry is ~1:1. In these conditions, the ICP0-RS4pm had six-fold higher STUbL activity as compared with ICP0-RS4 (Fig. 6F and G).

The STUbL activity of ICP0 was also compared with its phosphomimetic form ICP0pm, using the SUMOylated PML or Sp100 as the substrates. FLAG-PML was SUMOylated, captured on anti-FLAG affinity beads, and washed. Subsequently, ubiquitination reaction was carried out on the beads using Ube1 (E1), Ube2d1 (E2), Alexa-Ub, and either ICP0 or ICP0pm as the E3. The reaction was quenched by EDTA after 30min and washed (3×), and the pellet was separated on SDS gel. The ICP0pm showed a 5-fold increase in STUbL activity

PMLs and Sp100s as the substrates, separated on SDS gel and blotted with anti-FLAG antibody. (C) SUMOylated PMLs was captured on anti-FLAG affinity beads, washed (3×), and used as substrates in ubiquitination reaction using Ube2d1 as the E2, Alexa-Ub, and either ICP0 or its mutants as the E3. After the reaction, beads were washed (3×), separated on SDS gel, and visualized in Uvitec (Cambridge). (D) Same as (C) using SUMOylated Sp100s. (E) SUMOylation reaction using GST-PML as the substrate. (F) Same as in (C), except the SUMOylated PML was captured on glutathione (GSH) beads. (G) Same as in (F), except that in one reaction (rightmost lane), SENP2 was added for 2 h to cleave the SUMO chains on PML before adding ICP0 and other components of ubiquitination reaction. (H) Schematic of the experiments used to detect if the poly-Ub chains are assembled on SUMO chains or the substrate PML. (I) The beads and elutes of (H) are separated on SDS gel and visualized. The (-ve) lanes in (C), (D), (F), (G), and (I) do not include the SUMO-activating enzyme SAE1/2. SUMO, small ubiquitin-like modifier; E3, ubiquitin ligase; ICP0, infected cell polypeptide 0; SAE, SUMO Activating Enzyme; SENP2, Sentrin-specific protease 2.

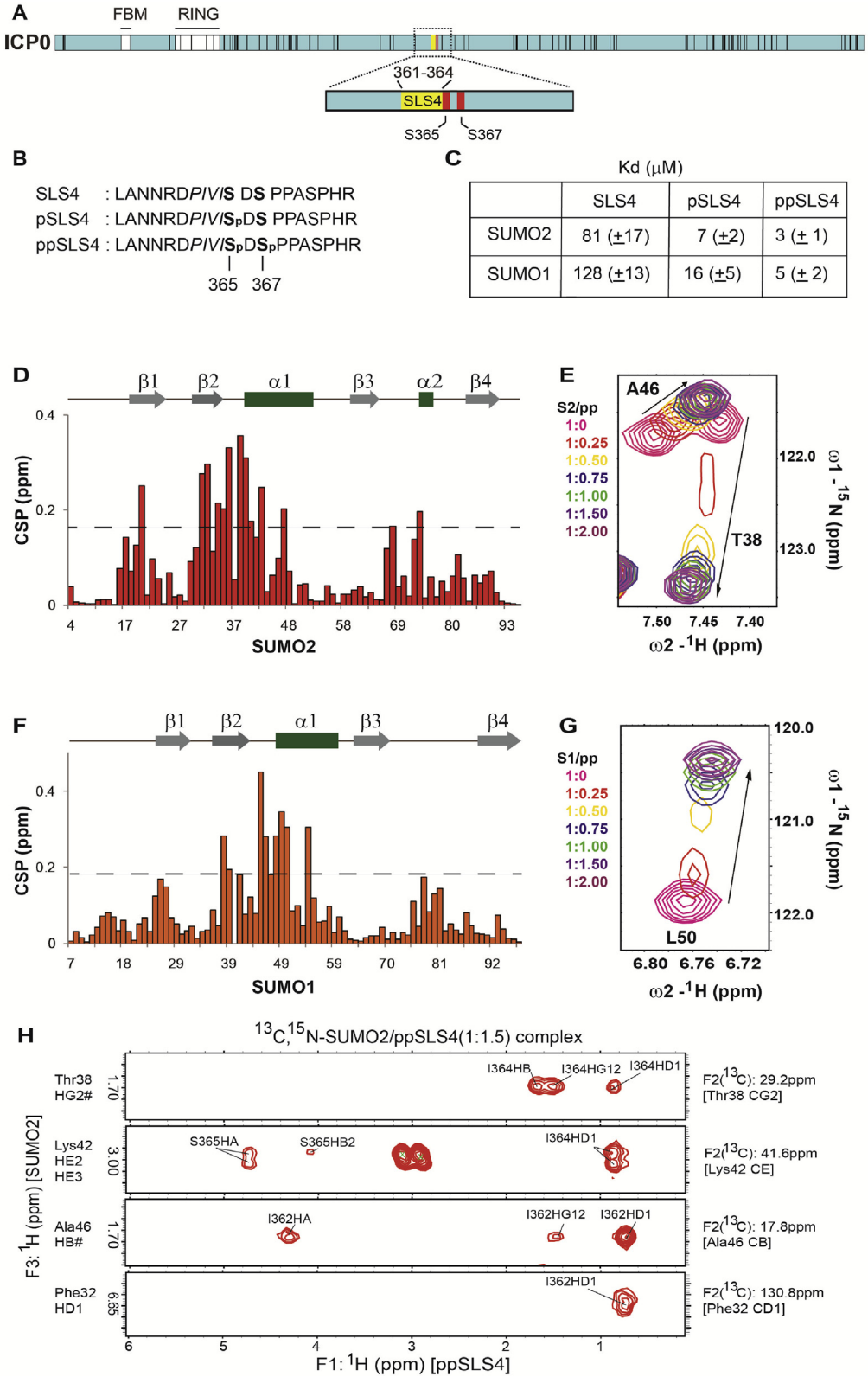

Fig. 5. ICP0 is phosphorylated at SLS4, which increases its affinity for SUMO. (A) Phosphorylation of ICP0 detected in HEK293T by mass spectrometry. All vertical black lines denote detected phosphorylation sites in ICP0. The region around SLS4 is expanded to show that only two serines immediately adjacent to SIM1 are phosphorylated. Ser365 and Ser367 are colored as red lines. (B) The sequence of the SLS4, pSLS4, and ppSLS4. (C) Dissociation constants of the binding of

Table 2. NMR and refinement statistics of the SUMO/ppSLS4 complexes.

NMR restraints and structural statistics	SUMO1/ppSLS4	SUMO2/ppSLS4
Unambiguous restraints (NOE)	55	53
Dihedral restraints (phi,psi)	18	18
HADDOCK parameters		
Cluster size	200	200
HADDOCK score	−143.6 (±3.9)	−115.6 (±3.6)
Van der Waals energy	−44.3 (±3.1)	−35.5 (±2.4)
Electrostatic energy	−623.2 (±8.9)	−525.7 (±11.5)
Restraints violation energy	+1.5 (±0.81)	+1.4 (±1.8)
Buried surface area	+1359.7 (±57.2)	+1220.2 (±38.2)
Rmsd[a] (Å)		
All backbone	0.5	0.3
All heavy atoms	0.7	0.6
Molprobity[b]		
Clash score	3.5	6.3
Score	2.2	2.1
Ramachandran statistics[b]		
Most favored regions	87.0	95.6
Allowed regions	10.4	4.4
Generous regions	1.3	0.0
Disallowed regions	1.3	0.0

SUMO, small ubiquitin-like modifier; SLS, SIM-like sequence; SIM, SUMO-interacting motif; ppSLS4, diphosphorylated SLS4; NMR, Nuclear Magnetic Resonance.
[a] Calculated for an ensemble of 20 lowest energy structures.
[b] Calculated for the lowest energy structure.

compared with the ICP0 (Fig. 6H and I). When Sp100s was used as the substrate, the effect of phosphorylation was similar (Fig. 6J and K). The ubiquitination of SUMOylated GST-PML was also enhanced in ICP0pm compared with apo ICP0 (Fig. 6L).

Kinetic analysis of the STUbL activity between ICP0 and ICP0pm can determine if phosphorylation increased the intrinsic activity of ICP0 or the affinity toward the substrate. A multiround ubiquitination kinetics experiments were carried out using either ICP0 or ICP0pm as the E3 and $(SUMO2)_n$ chains on SUMO affinity beads as the substrate. The reactions were quenched with excess EDTA at different time points, washed, separated on SDS gel, and quantified (Fig. 6M and N). The measured ubiquitination rates of ICP0pm were higher than the ICP0 (Fig. 6O). A comparison of the kinetic parameters between ICP0 and ICP0pm indicated that phosphorylation did not affect the Kcat of the reaction but reduced the Km for the substrate by 4-fold (Fig. 6P). Altogether, phosphorylation of ICP0 at SLS4 increases its affinity for SUMOylated substrates and consequently its STUbL activity.

Chk2 binds to ICP0 and phosphorylates SLS4

Previous research study has indicated that the ATM-Chk2 pathway is important for HSV-1 growth [18]. The effect of Chk2 inhibition on HSV-1 replication was tested. Vero cells were infected with HSV-1 17 syn + at the multiplicity of infection (MOI) of 0.1 in the presence and absence of Chk2 inhibitor. Infection in the presence of Chk2 inhibitor exhibits slower progression of cytopathic effect (CPE) as compared with the infection in the untreated sample (Fig. S13A). HSV-1−mediated cell rounding and detachments were significantly retarded in the presence of Chk2 inhibitor at 36, 48, and 60 hours post-infection (hpi), suggesting that Chk2 inhibition is detrimental to the HSV-1 growth. Virus yield was determined by plaque assay in Vero cells. Chk2-inhibited cells yielded approximately 1000-fold less virus at 48 and 60 hpi than the

SUMO with SLS4, pSLS4, and ppSLS4. ppSLS4 induced CSPs observed in SUMO2 and SUMO1 are plotted in (D) and (F), respectively. (E) and (G) show a typical amide resonance that undergoes intermediate exchange when SUMO2 (S2/pp) and SUMO1 (S1/pp) bind ppSLS4, respectively. (H) Selected strips from the ^{13}C, ^{15}N-filtered (F1), ^{13}C, ^{15}N-edited (F2) NOESY HSQC spectra are depicting intermolecular NOEs between ^{13}C-bonded protons of ^{13}C, ^{15}N-labeled SUMO2, and unlabeled ppSLS4. ^{13}C and ^{1}H assignment of SUMO2 atoms are given on the right and left of the strips, respectively. The protons of SLS4 that show NOEs to SUMO2 are labeled. ICP0, infected cell polypeptide 0; SUMO, small ubiquitin-like modifier; SLS, SIM-like sequence; SIM, SUMO-interacting motif; ppSLS4, diphosphorylated SLS4; CSPs, chemical shift perturbations; HSQC, heteronuclear single quantum coherence.

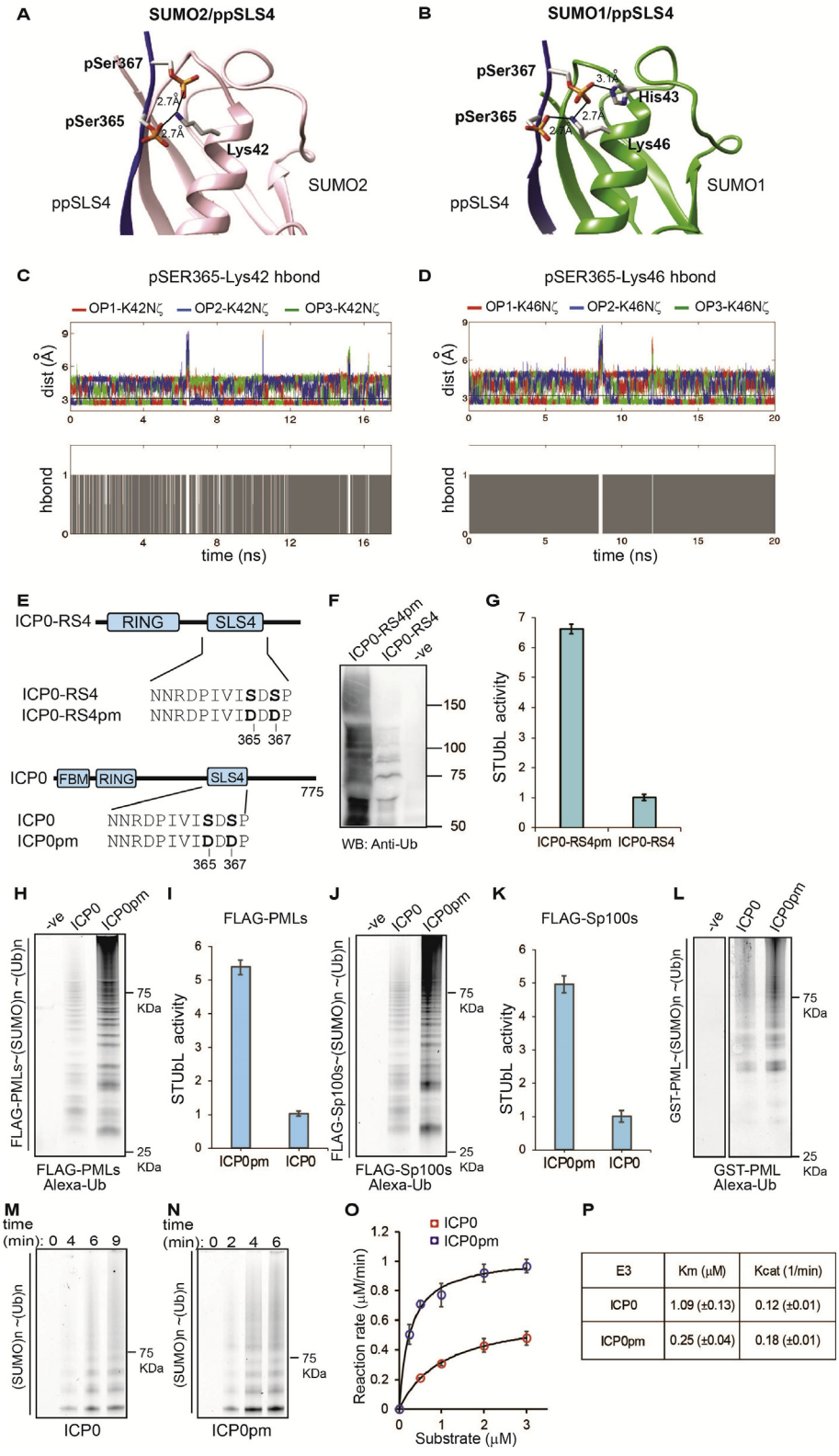

E3	Km (μM)	Kcat (1/min)
ICP0	1.09 (±0.13)	0.12 (±0.01)
ICP0pm	0.25 (±0.04)	0.18 (±0.01)

Fig. 6. Phosphorylation of SLS4 creates new hydrogen bonds at the SUMO/SLS4 interface to increase the STUbL activity of ICP0. (A) and (B) show the lowest energy structures of SUMO2/ppSLS4 and SUMO1/ppSLS4 complexes, respectively. The hydrogen bonds between phosphorylated side chains of SLS4 and SUMO1/2 are shown as black lines. (C) Distances between the three phosphate oxygen atoms of pSer365 and lysine 42 Nζ of SUMO2 are plotted against time

untreated cells, confirming that Chk2 promotes viral growth (Fig. 7A).

CK1 phosphorylates ICP0 at Thr67 in the Forkhead Associated -binding motif (FBM, aa: 55−74) in ICP0 (Fig. 1A). Upon phosphorylation, ICP0 interacts with FHA domains [32]. Because Chk2 phosphorylates serines, promotes HSV replication, and includes an FHA domain, it can potentially bind and phosphorylate ICP0 (Fig. 7B). This hypothesis was tested with various tools. The interaction of the phosphorylated FBM with the Chk2-FHA domain was studied by Isothermal Titration Calorimetry. The binding isotherm given in Fig. 7C indicated a strong interaction between FBM and Chk2-FHA. The dissociation constant was measured to be 750 nM, consistent with a previous measurement of the FHA/FBM interaction [32].

A sample of ^{13}C, ^{15}N-Chk2-FHA was prepared to obtain molecular details of this interaction by NMR. The backbone chemical shifts of the Chk2-FHA domain were assigned using 3D HNCO, HN(CA)CO, HNCA, and HN(CO)CA experiments (Fig. S14A). A synthesized peptide of FBM was titrated into the sample of ^{13}C, ^{15}N-Chk2-FHA. At 1:0.5 stoichiometric ratio of Chk2-FHA:FBM, the spectra of Chk2-FHA showed a new set of resonances coming from the FBM bound conformation of Chk2-FHA apart from the resonances of the free Chk2-FHA. The simultaneous presence of resonance peaks corresponding to both free and bound conformations indicated that the peaks are in slow exchange compared with the NMR timescale. The slow exchange is a signature of a strong interaction between FBM and the Chk2-FHA, which corroborates the ITC data. At 1:1.2 stoichiometric ratio of Chk2-FHA:FBM, only the peaks corresponding to bound conformation remained in the spectra, implying that Chk2-FHA is saturated with FBM. Fig. 7D shows the overlay of free and bound Chk2-FHA. The bound spectra were reassigned using standard 3D NMR experiments. Significant amide CSPs were observed between the free and the bound form of the Chk2-FHA domain (Fig. S14B). However, Chk2 precipitated at high concentrations (0.2 mM), and further 3D experiments for assigning resonances from side chains atom and intermolecular NOESY experiments were not feasible. Hence, the CSPs were used to dock the FBM to the Chk2-FHA domain (PDB ID: 1GXC) by HADDOCK [23]. Table 3 provides the statistics of the docked structures. Fig. 7E shows the lowest energy structural model of the Chk2-FHA/FBM complex. The surface representation in Fig. 7E shows how the CSPs correlate with the FBM interface on the Chk2-FHA domain.

The Chk2-FHA domain has a beta-sandwich fold composed of 8 beta strands. The N-termini and the C-termini beta strands align together to form a compact and independent modular domain. The loop between β2 and β3 is extended and also contains a short alpha helix. The phosphorylated FBM binds to the loops between the beta strands β2/β3, β4/β5, and β7/β8 (Fig. 7E). Phosphorylation of Thr67 appears to be essential for this interaction as the phosphate group forms multiple hydrogen bonds with the basic residues in the β2/β3 loop: (i) side chain of Arg117, (ii) side chain of Lys141, and (iii) backbone of Lys141 (Fig. 7F). T67 also forms hydrogen bonds with the side chain of Ser140 (Fig. 7F). Leu193 in the β7/β8 loop forms several hydrophobic contacts with the aromatic ring of Phe70 in FBM (Fig. S14C). A couple of the FHA-CHk2 residues interact with the backbone of the FBM and help to stabilize the polypeptide at the interface. For example, Asn166 in the β4/β5 loop forms two hydrogen bonds with the backbone of Glu68 and Phe70 of FBM (Fig. S14C). Similarly, Lys141 side chain Nζ forms a hydrogen bond with the Thr65 backbone oxygen atom (Fig. 7F).

After confirming Chk2-FHA/ICP0-FBM binding, the phosphorylation of ICP0 at SLS4 was checked

in the MD simulation. Given below is the presence/absence of the hydrogen bond between any one of the phosphorus atoms of pSer365 and lysine 42 Nζ digitized to a two-stage process (0 or 1), and plotted against time. (D) Similar to (C) plotted for the distance between phosphorylated Ser365 and lysine 46 Nζ of SUMO1. (E) Schematic of ICP0-RS4, ICP0, and the phosphomimetic version ICP0-RS4pm and ICP0pm. (F) Ubiquitination assays using ICP0-RS4 and the phosphomimetic ICP0-RS4pm as the E3 and SUMO2 chains as the substrate carried out on SUMO2 affinity beads, washed and blotted with the anti-Ub antibody. The (-ve) control lane in this assay lacks the E3. (G) Quantification of the bands observed in (G), where the intensity of ICP0-RS4 lane is normalized to 1. The values are mean of three reactions, and the standard deviation is plotted as error bars. (H) Ubiquitination reaction using SUMOylated PMLs as in Fig. 4C, using ICP0 and ICP0pm as the E3 here. (I) The lanes in (H) are quantified and plotted. (J) Same as in (H) using SUMOylated Sp100s as the substrate and quantified in (K). (L) Same as in Fig. 4F, using ICP0 and ICP0pm as the E3. (M) Multiround ubiquitination reaction as performed in Fig. 3I, using 0.5 μM $(SUMO)_n$ as the substrate and ICP0 as the E3. The reaction is quenched at different time points (0min, 4min, 6min, and 9min) by adding EDTA and separated on SDS gel. (N) Same as in (M) using ICP0pm as the E3. The time points are (0min, 2min, 4min, and 6min). (O) The reaction rates of ICP0 and ICP0pm are compared at the different substrate [$(SUMO2)_n$] concentrations. The values are the mean of triplicates, and the error is the standard deviation of the same. The fit of the data to the Michelis-Menten equation is given as black lines. (P) The kinetic parameters of STUbL activity for ICP0 and ICP0pm are given in a table. The values are the mean of triplicates, and the error is the standard deviation of the same. E3, ubiquitin ligase; SUMO, small ubiquitin-like modifier; SLS, SIM-like sequence; SIM, SUMO-interacting motif; STUbL, SUMO-targeted ubiquitin ligase; ICP0, infected cell polypeptide 0; ppSLS4, diphosphorylated SLS4; MD, molecular dynamics; PML, Promyelocytic leukemia protein.

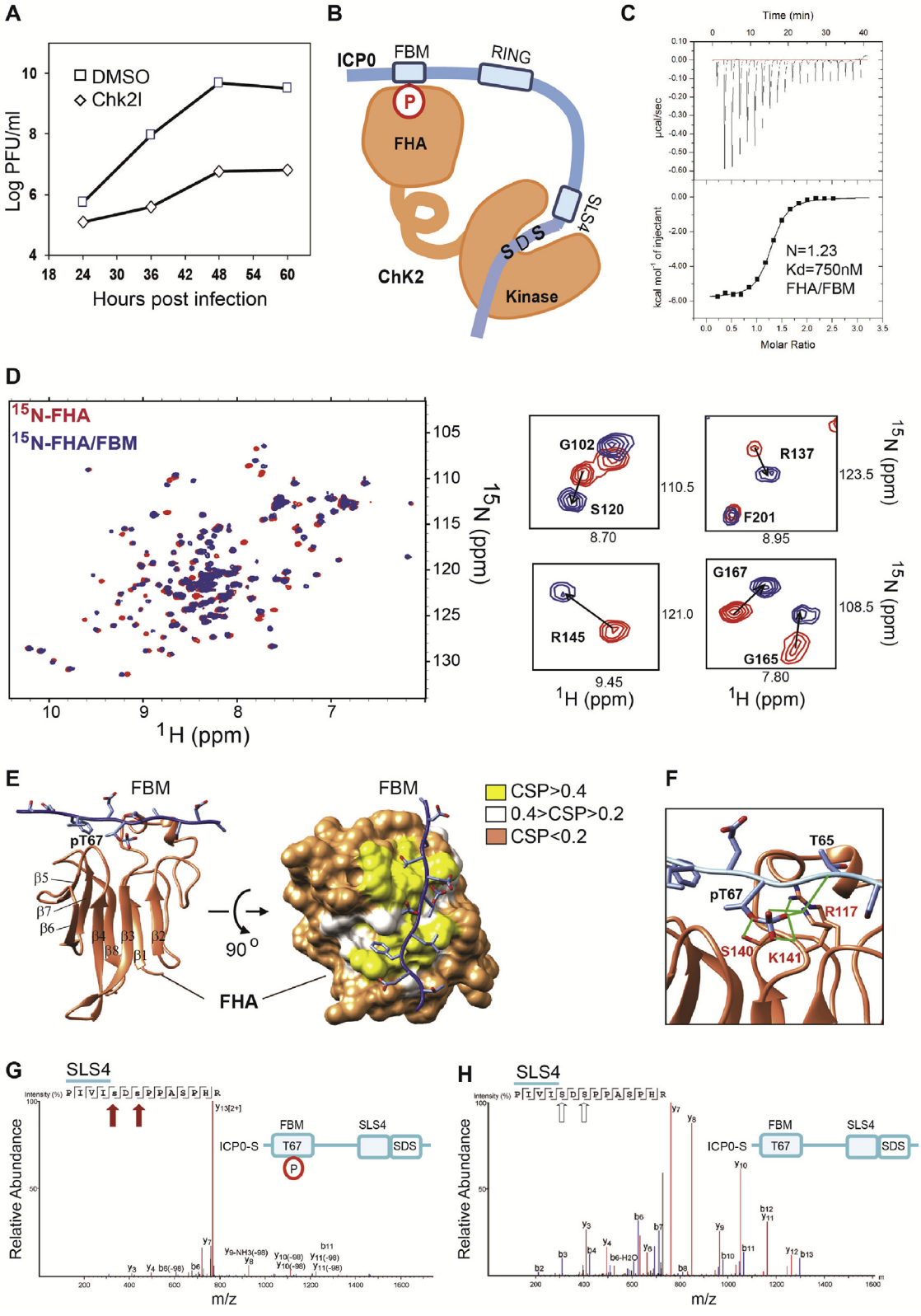

Fig. 7. Chk2 interacts with ICP0 and phosphorylates SLS4. (A) Chk2 inhibition suppresses HSV-1 replication. Vero cells were infected at MOI of 0.1 using HSV-1 17 syn + as described in material and methods. Mock treatment (DMSO) was included as a negative control. Cells and medium were harvested at the indicated time points, and virus yield was assessed by the plaque assay in Vero cells. The values are mean of three experiments. The standard deviation at each

Table 3. NMR and refinement statistics of the Chk2-FHA/ICP0-FBM complex.

NMR restraints and structural statistics	Chk2-FHA/ICP0-FBM
Ambiguous restraints	
Active	8
Passive	10
HADDOCK parameters	
Cluster Size	108
HADDOCK score	−69.9 (±20.9)
Van der Waals energy	−44.3 (±3.1)
Electrostatic energy	−14.4 (±6.8)
Restraints violation energy	+1.0 (±0.7)
Buried surface area	+767.6 (±113.7)
Rmsd[a] (Å)	
All backbone	1.3
All heavy atoms	1.4
Rmsd[a] (Å) (ordered region)[c]	
All backbone	0.6
All heavy atoms	0.9
Molprobity[b]	
Clash score	5.8
Score	2.3
Ramachandran statistics[b]	
Most favored regions	87.3
Allowed regions	13.5
Generous regions	1.0
Disallowed regions	1.9

FBM, FHA-binding motif; ICP0, ICP0, infected cell polypeptide 0; NMR, Nuclear Magnetic Resonance.
[a] Calculated for an ensemble of 20 lowest energy structures.
[b] Calculated for the lowest energy structure.
[c] Ordered residues Chk2: 92−207, ICP0: 65-70.

by MS/MS analysis. A synthetic peptide was designed where the two ICP0 motifs FBM and SLS4 were fused with an intermediate stretch of ~30 wild-type residues (total 45 residues) to test whether Chk2 can phosphorylate SLS4. Thr67 is phosphorylated in ICP0−S to promote FHA/FBM binding. The chimera is shown in Fig. 7G and referred to as ICP0−S. A phosphorylation reaction was initiated with Chk2 as the kinase and the ICP0−S as the substrate. After the reaction, the phosphorylation status of Ser365 and Ser367 was determined by trypsin digestion followed by MS/MS analysis. The mass of peptide fragments corresponding to SLS4 shows that Chk2 phosphorylated SLS4 at both Ser365 and Ser367 (Fig. 7G). Some SLS4 was observed where only the Ser367 is phosphorylated (Fig. S15A), indicating that Chk2 initially phosphorylates Ser367, followed by Ser365. SLS4 phosphorylation was not detected when the ICP0−S is unphosphorylated at Thr67 (Fig. 7H). When the phosphorylation of SLS4 containing fragment in ICP0 was compared between control and Chk2-inhibited cells, the phosphorylation dropped by 60% (Fig. S16, S17 and S18). The remnant phosphorylation despite inhibition could be due to another kinase that also targets SLS4. Further studies with multiple kinases are required to identify other kinases that may also be involved.

time point is minor and hence plotted separately in Fig. S13B. (B) A proposed phosphorylation mechanism of phosphoserines near SLS4, which is dependent on the interaction between the Chk2-FHA domain and the phosphorylated FBM from ICP0. (C) ITC binding data of FHA/FBM interaction. The titration curve indicates an exothermic reaction with the dissociation constant Kd = 750 (±50) nM, stoichiometry = 1.23, ΔH = −5.8 (±0.1)kcal/mol, and ΔS = 8.5cal/(K.mol.T). (D) An overlay of the ^{15}N-edited HSQC of free ^{15}N-labeled FHA domain in red and the ^{15}N-FHA:FBM (1:1.2) in blue. Expanded regions of the spectra are given on the right. (E) The NMR data guided the HADDOCK structure of the Chk2-FHA/FBM complex. A surface representation of the complex showing observed CSPs on the surface of the FHA domain. (F) The hydrogen bonds observed between FHA and FBM around phosphorylated T67. The hydrogen bonds are colored in green. (G) Schematic of ICP0−S phosphorylated at Thr67, and the MS/MS spectrum of a tryptic peptide of Chk2 treated ICP0−S. The MS/MS data confirm that Chk2 phosphorylates ICP0−S at the phosphoserines S365 and S367 near SLS4 (red arrows). (H) The MS/MS data of Chk2 treated ICP0−S that is not phosphorylated at Thr67 phosphorylation. The serines are not phosphorylated in this case (white arrows). SLS, SIM-like sequence; SIM, SUMO-interacting motif; ICP0, infected cell polypeptide 0; CSPs, chemical shift perturbations; HSV-1, HSV-1, herpes simplex virus-1; NMR, Nuclear Magnetic Resonance.

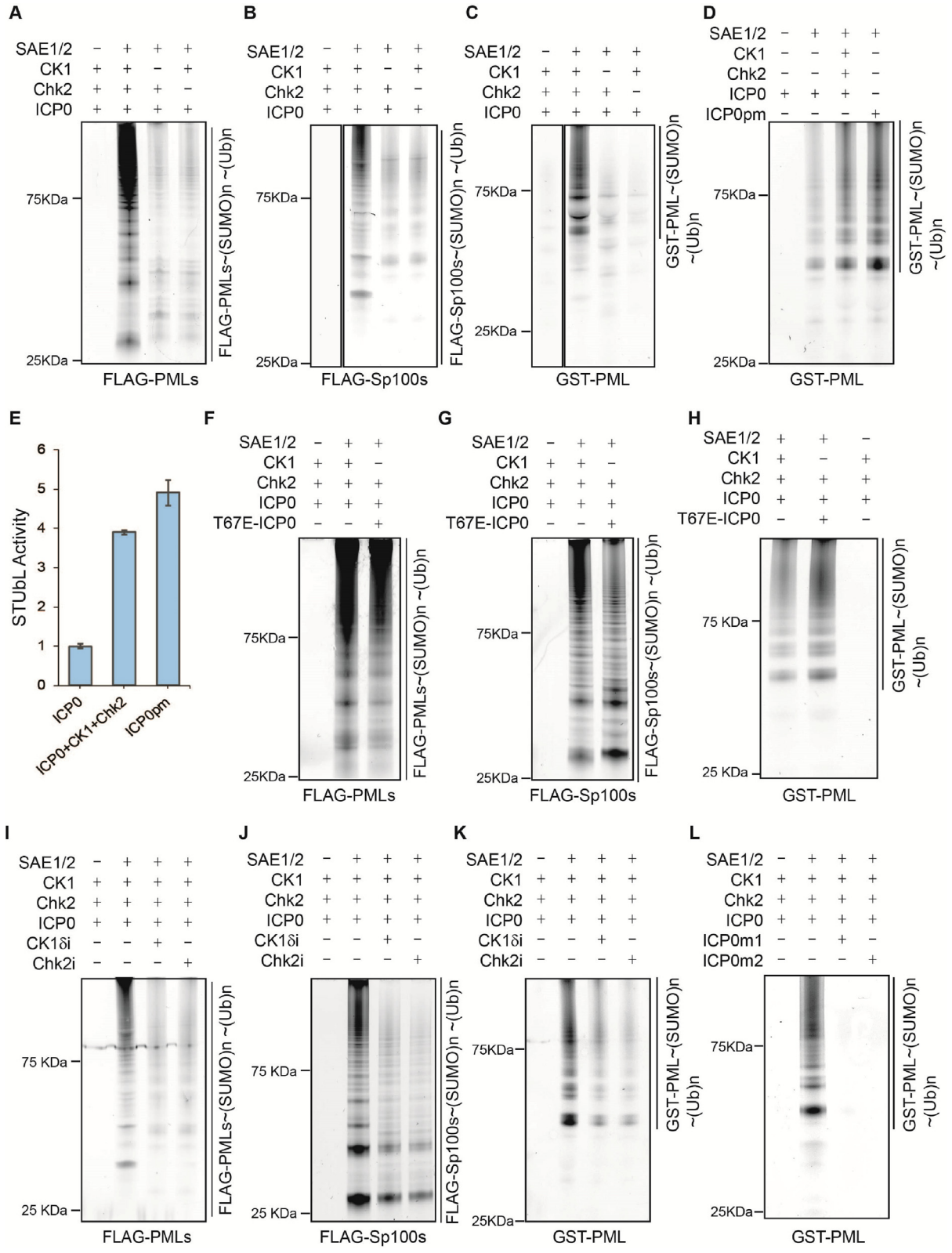

Fig. 8. CK1 and Chk2 treated ICP0 has enhanced STUbL activity. Ubiquitination of SUMOylated (A) FLAG-PMLs, (B) FLAG-Sp100s, and (C) GST-PML was carried out as in Fig. 4, except that ICP0 was pretreated with either CK1 or Chk2 or both before the start of the ubiquitination reaction. (D) The activation of ICP0 by CK1 and Chk2 was compared with the phosphomimetic mutant ICP0pm, using GST-PML as the substrate. The ubiquitinated bands were quantified and plotted in

Several phospho-SIMs have been identified where phosphorylation is carried out by CK2. PML degradation by ICP0 is not modulated by CK2 [33], implying that it may not target SLS4. A comparison of CK2 target phospho-SIMs with SLS4 shows that although the N-terminal sequence of ICP0 SLS4 is similar to other phospho-SIMs, the C-terminal sequence is different (Fig. S15B). The C-terminal region is acidic in other phospho-SIMs but proline-rich in ICP0 SLS4. Such differences may explain why CK2 is not relevant for PML degradation. Overall, upon phosphorylation of ICP0 at Thr67 by CK1, Chk2 binds and phosphorylates ICP0 at SLS4.

CK1 and Chk2 work in tandem to increase the STUbL activity of ICP0

The phosphorylation at SLS4 should increase the STUbL activity of ICP0. The effect of CK1 and Chk2 on the STUbL activity of ICP0 was measured using the substrates used previously. The sequential treatment of ICP0 by CK1 and Chk2 increased its STUbL activity for PMLs, Sp100s, and PML (Fig. 8A–C). The STUbL activity of CK1 and Chk2 treated ICP0 was similar to the activity of phosphomimetic ICP0pm, indicating that the cumulative effect of CK1 and Chk2 treatment on the STUbL activity is the phosphorylation of SLS4 (Fig. 8D and E). A variant T76E-ICP0 was purified, which mimicked the phosphorylation at T67 by CK1. The STUbL activity of T67E-ICP0 treated with Chk2 alone, compared well with the activity CK1 and Chk2 treated ICP0 for PMLs, Sp100s, and PML (Fig. 8F–H). The effect of CK1 inhibitors (CK1i) and Chk2 inhibitors (Chk2i) on the STUbL activity of ICP0 was tested. During the phosphorylation reaction, either CK1i or Chk2i was added in the reaction mix. The inhibition of either CK1 or Chk2 depleted the STUbL activity of ICP0 for PMLs, Sp100s, and PML (Fig. 8I, J, and 8K), which indicated that both the kinases were required for SLS4 phosphorylation. However, phosphorylation of ICP0 by CK1 and Chk2 could not rescue the STUbL activity of hydrophobic and charge mutants, suggesting that those residues are central to the SUMO/SLS4 interaction (Fig. 8L). Altogether, these results suggest that CK1 and Chk2 act on ICP0 in tandem and enhance its STUbL activity.

Discussion

ICP0 is transcribed during the immediate early stages of the lytic cycle, and one of its key functions is to degrade PML NBs and alleviate host-induced transcriptional repression [34]. This process is critically dependent on the STUbL activity of ICP0, by which it can target SUMOylated proteins, assemble polyubiquitin chains on them, and tag them for proteasomal degradation. One or more of the SLS regions in ICP0 are expected to target SUMOylated proteins. Several cellular studies have indicated the importance of the region around SLS3 and SLS4 for the degradation of the PML NBs [16,35–37] [38]. However, the C-terminal region, including SLS5-7, was also shown to be important for PML NB degradation [39]. Precisely which of these SLS regions is the bona fide SIM and targets SUMOylated proteins was unclear. Here, a comprehensive study of all the SLS regions identified SLS4 as the sole bona fide SIM in ICP0. NMR titrations showed that the other SLS regions do not bind SUMOs. Moreover, the entire region of SLS5-7 did not bind to SUMO, which does not correlate with the relevance of SLS5-7 for PML NB degradation. A recent study postulated that SLS5-7 could be a portion of a larger structural fold [16]. Our results strengthen the possibility that SLS5-7 constitutes a structural fold that either binds SUMOs or other PML NB constituent proteins via a mechanism that is entirely different from the typical SUMO/SIM interaction.

From the sequence of SLS regions, it is unclear why SUMO interacts exclusively with SLS4 and not the other SLS regions. The structural model of SUMO/SLS4 complexes provided the underlying mechanism. The structures suggest that both hydrophobic and electrostatic interactions are critical for the SUMO/SLS4 binding. SUMO1 and SUMO2 include an exposed hydrophobic shallow groove between β2 and α1. The two isoleucines Ile362 and Ile364 in SLS4 bury their side chains into this groove and form extensive hydrophobic contacts with SUMO1 and SUMO2. In addition, the two aspartic acids Asp360 and Asp366 make ionic interactions with the basic residues of β2 and α1. The other SLS sequences do not have the combination of these hydrophobic and acidic residues in the proper arrangement. Hence, they do not bind SUMO1 or

(E). The values are a mean of three experiments, while the error is the standard deviation of the same. (F) The STUbL activity was compared between CK1+Chk2 treated ICP0 and a phosphomimetic mutant T67E-ICP0, which mimics the phosphorylation of ICP0 by CK1. Here, FLAG-PML was used as the substrate. FLAG-Sp100s and GST-PML were used as the substrate in (G) and (H). The STUbL activity of CK1 and Chk2 treated ICP0 was compared with its STUbL activity in the presence of either the CK1 inhibitor (CK1i) or the Chk2 inhibitor (Chk2i). ICP0 was treated with CK1, Chk2, and either the CK1i or Chk2i before using it for ubiquitination of SUMOylated PMLs. The same reactions were also carried out using (J) FLAG-Sp100s and (K) GST-PML as the substrate. (L) The SLS4 mutants ICP0m1 and ICP0m2 were treated with CK1 and Chk2 and used for the ubiquitination of SUMOylated GST-PML. Their activity was compared with CK1, Chk2 treated wt-ICP0. The Ub used in all the assays in this figure is Alexa-Ub and the CK1 isoform used is CK1δ. SUMO, small ubiquitin-like modifier; SLS, SIM-like sequence; SIM, SUMO-interacting motif; ICP0, infected cell polypeptide 0; STUbL, SUMO-targeted ubiquitin ligase; PML, Promyelocytic leukemia protein.

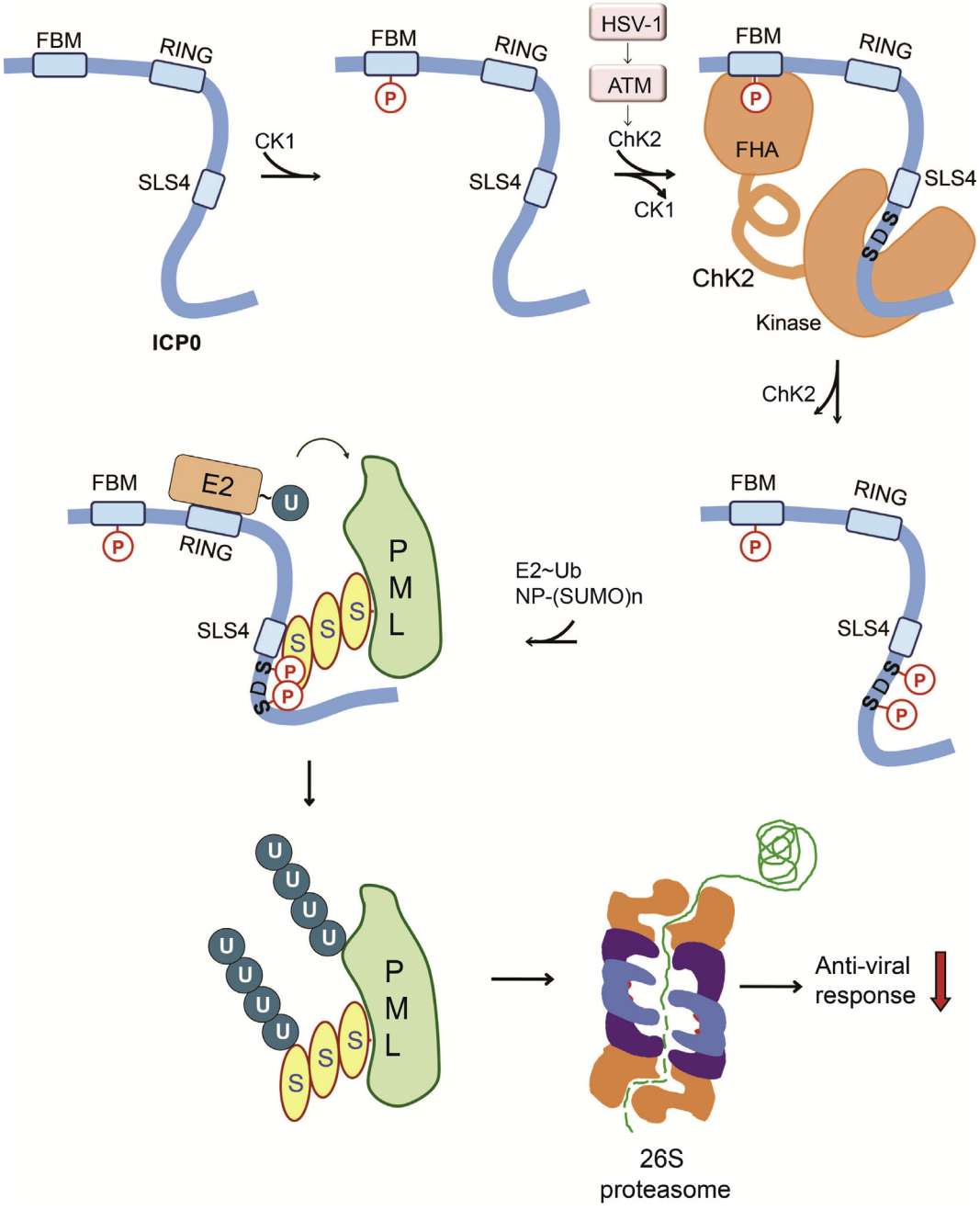

Fig. 9. The proposed model for Chk2-mediated activation of ICP0. CK1 phosphorylates the N-terminal FBM at Thr67. HSV-1 activates the ATM-Chk2 pathway, and the activated Chk2 binds ICP0 to phosphorylate the phosphoserines at SLS4. The phosphorylated ICP0 identifies SUMOylated nuclear proteins such as PML with higher affinity and assembles polyubiquitin chains using the E2~Ub to tag them for degradation by the 26S proteasome. SUMO, small ubiquitin-like modifier; SLS, SIM-like sequence; SIM, SUMO-interacting motif; ICP0, infected cell polypeptide 0; HSV-1, herpes simplex virus-1; PML, Promyelocytic leukemia protein; Ataxia–telangiectasia-mutated kinase, ATM; Checkpoint kinase 2, Chk2.

SUMO2. The loss of STUbL activity upon mutations at the SUMO/SLS4 interface underlines the functional importance of this interaction.

Phosphorylation of viral proteins is important for lytic reactivation in the Herpesviridae family [40–43]. Phosphorylation of ICP0 is vital for PML NB disruption [30,31]. Specifically, HSV-1 is defective in neuronal replication and explant-induced reactivation from latency when Ser365, Ser367, and Ser371 are mutated to alanines in ICP0 [31]. For reasons unknown, the mutant was also unable to degrade SUMOylated PML from the PML NBs [30]. Ser371 is

far from the binding interface to create an impact on the SUMO/SLS4 binding. However, phosphorylation of Ser365 and Ser367 dramatically increased the SUMO/SLS4 affinity by ~25 fold and the STUbL activity of ICP0 by six-fold (Figs. 5 and 6). PML NBs are short-lived post association with ICP0. Although SUMO/SLS4 affinity is weak, a couple of factors may help ICP0 to degrade PML NBs rapidly. First, the constitutive proteins in PML NBs such as PML, Sp100, and hDaxx are heavily SUMOylated, leading to a high local concentration of SUMO in the PML NBs. The high local concentration would drive ICP0 to specifically target PML NBs over other SUMOylated proteins in the nucleus. Second, phosphorylation at SLS4 increases the affinity of ICP0 for SUMOylated proteins. Third, SLS4 phosphorylation also enhances the STUbL activity of ICP0. These factors may act synergistically to activate ICP0 into a potent STUbL that is specific for PML NBs. The importance of phosphorylation is highlighted by the fact that a mutant ICP0 that cannot be phosphorylated at SLS4 is defective in degrading PML NBs [30].

Cross-talk between PTM signaling is a known trend in eukaryotic biology [44]. For example, phosphorylation can increase and inhibit ubiquitination [44–46]. SUMOylation and ubiquitination can compete for the same lysine in a protein [47]. Phosphorylation can promote SUMOylation through the phosphorylation-dependent SUMOylation motif [48]. In some proteins such as c-Myb, phosphorylation can also inhibit SUMOylation [49]. The phosphorylation regulated SUMO/SIM affinity has been observed in both host and viral proteins [50,51]. Until now, these three PTMs were found to cross-talk in a pair-wise manner. In this study, we find that phosphorylation increases the activity of ubiquitin ligase in a SUMO-dependent manner (Fig. 9). Kinetic assays demonstrate that the affinity of ICP0 for SUMOylated substrates increases upon phosphorylation, switching it into a potent STUbL. To our knowledge, this is the first instance where all three PTM signaling pathways ubiquitination, SUMOylation, and phosphorylation are simultaneously involved in a cross-talk. SIMs in several other STUbLs such as Uls1, Slx5, Slx8 (*S. Cerevisiae*), Rfp1 (*S. pombe*), Rad18 (*H. Sapiens*), and Arkadia (*H. Sapiens*) have phosphoserines nearby [14,24]. It remains to be seen whether phosphorylation-regulated STUbL activity is prevalent in the eukaryotic E3s or is exclusive to the viral E3s.

Viruses often pack multiple functions into a single viral gene. Our results highlight that the virus can also use a single host protein for multiple functions. HSV-1 both activates and is dependent on the ATM-Chk2 pathway for an effective infection [34]. Chk2 is essential for the cell cycle arrest at the G2/M phase [18]. We show that besides regulating cell cycle arrest, ICP0 also exploits Chk2 to phosphorylate SLS4 and activate itself for degradation of antiviral responses (Fig. 9). Inhibition of Chk2 significantly retarded CPE progression of HSV-1 and reduced the viral growth by 1000-fold. *In-vitro* phosphorylation reactions revealed that Chk2 phosphorylates SLS4. In addition, structural studies provide atomistic details of the direct interaction between ICP0 and Chk2. Cellular studies also confirmed that Chk2 inhibition reduces phosphorylation at SLS4. The phosphorylation of Chk2 is dependent on CK1, which is activated during infection as a part of the host immune response [52]. The in-tandem action of CK1 and Chk2 could be necessary to regulate ICP0 activity during infection.

As a part of the antiviral response, rescue factors such as RNF8 assemble at the viral replication nodes to inhibit transcription of the viral genome. Upon phosphorylation by CK1 at the FBM region, ICP0 binds to the RNF8-FHA domain and degrades RNF8 [32]. Similarly, the Chk2-FHA domain also binds to ICP0 and Chk2 activates ICP0 to degrade PML NB proteins. Interestingly, while RNF8 degradation occurs in a SUMO-independent manner, degradation of SUMOylated PML NB proteins occurs in a SUMO-dependent mechanism. Given both the host antiviral responses (RNF8 and PML NBs) are negated by the FHA/FBM interaction, this interaction now becomes an interesting target for therapeutic intervention. Evidently, the viral E3 ICP0 has developed a meticulous strategy to modulate the host antiviral responses for efficient viral replication. We find that the cross-talk between multiple PTMs plays a vital role in its strategy.

Accession Numbers

The coordinates of SUMO2/SLS4 and SUMO1/SLS4 are deposited in the PDB under accession codes 6JXW and 6JXU, respectively. The coordinates of SUMO2/ppSLS4 and SUMO1/ppSLS4 were deposited in the PDB under accession codes 6JXX and 6JXV, respectively. The backbone assignments of the Chk2 FHA domain were deposited in Biological Magnetic Resonance Bank under accession code 27042.

Acknowledgments

The Nuclear Magnetic Resonance (NMR) data were acquired at the National Centre for Biological Science-Tata Institute of Fundamental Research NMR Facility. The authors would like to thank Purushotham Reddy for helping with NMR data acquisition. The MS data were collected at VProteomics (New Delhi) and at National Centre for Biological Science Proteomics facility. The SUMO1

plasmid was a gift from Rama Koti (Tata Institute of Fundamental Research). Chk2-FHA plasmid was kindly provided by Ashok Venkitaraman (InStem). R. Andrew Byrd (NCI) and Allan Weissman (NCI) are acknowledged for critical comments on the manuscript. H.N is supported by a fellowship from Council of Scientific and Industrial Research-University Grants Comission, Government of India. R.D. is the recipient of Ramalingaswamy fellowship from the Department of Biotechnology (DBT), Government of India. This research was funded by intramural grants from the National Center for Biological Sciences, Tata Institute of Fundamental Research.

Author contribution

Dambarudhar SS Hembram:Investigation, Data curation, Validation, Writing- Original draft preparation. **Hitendra Negi**:Investigation, Methodology. **Poulomi Biswas**:Investigation, Methodology. **Vasvi Tripathi**:Investigation, Methodology. **Lokesh Bhushan**:Investigation, Methodology. **Divya Shet**:Investigation. **Vikas Kumar**:Investigation. **Ranabir Das**:Conceptualization, Fund acquisition, Investigation, Methodology, Writing- Original draft preparation, Writing- Reviewing and Editing.

Appendix A. Supplementary data

Supplementary data to this article can be found online at https://doi.org/10.1016/j.jmb.2020.01.021.

Received 6 October 2019;
Received in revised form 6 January 2020;
Accepted 17 January 2020
Available online 27 January 2020

Keywords:
ubiquitination;
SUMOylation;
phosphorylation;
host-virus interactions;
NMR spectroscopy

†Current address: Indian Institute of Technology, Kharagpur.

‡ Current address: Raman Research Institute, Bangalore.

§ Current address: University of Nebraska Medical Center, Omaha, NE.

References

[1] C.A. Ascoli, G.G. Maul, Identification of a novel nuclear domain. J. Cell Biol. 112 (5) (1991) 785–795. Available at: http://www.ncbi.nlm.nih.gov/pubmed/1999457%5Cnhttp://www.pubmedcentral.nih.gov/articlerender.fcgi?artid=PMC2288866.

[2] N. Stuurman, et al., A monoclonal antibody recognizing nuclear matrix-associated nuclear bodies. J. Cell Sci. 101 (4) (1992) 773–784.

[3] V. Lallemand-Breitenbach, H. de Thé, PML nuclear bodies. Cold Spring Harbor Perspect. Biol. 2 (5) (2010) 1–17, https://doi.org/10.1101/cshperspect.a000661.

[4] S.F. Banani, et al., Compositional control of phase-separated cellular bodies, Elsevier Inc. Cell 166 (3) (2016) 651–663, https://doi.org/10.1016/j.cell.2016.06.010.

[5] R.D. Everett, et al., PML contributes to a cellular mechanism of repression of herpes simplex virus type 1 infection that is inactivated by ICP0, J. Virol. 80 (16) (2006) 7995–8005, https://doi.org/10.1128/JVI.00734-06.

[6] R.D. Everett, M.K. Chelbi-Alix, PML and PML nuclear bodies: implications in antiviral defence, Biochimie 89 (6–7) (2007) 819–830, https://doi.org/10.1016/j.biochi.2007.01.004.

[7] R.D. Everett, DNA viruses and viral proteins that interact with PML nuclear bodies, Oncogene 20 (49) (2001) 7266–7273, https://doi.org/10.1038/sj.onc.1204759.

[8] N. Tavalai, T. Stamminger, Interplay between herpesvirus infection and host defense by PML nuclear bodies, Viruses 1 (3) (2009) 1240–1264, https://doi.org/10.3390/v1031240.

[9] G.G. Maul, H.H. Guldner, J.G. Spivack, Modification of discrete nuclear domains induced by herpes simplex virus type 1 immediate early gene 1 product (ICP0). J. Gen. Virol. 74 (Pt 12(May) (1993) 2679–2690, https://doi.org/10.1099/0022-1317-74-12-2679.

[10] M.K. Chelbi-alix, H. De The, Herpes virus induced proteasome-dependent degradation of the nuclear bodies-associated PML and Sp100 proteins, Oncogene 18 (1999) 935–941.

[11] J. Parkinson, R.D. Everett, Alphaherpesvirus proteins related to herpes simplex virus type 1 ICP0 affect cellular structures and proteins, J. Virol. 74 (21) (2000) 10006–10017, https://doi.org/10.1128/JVI.74.21.10006-10017.2000.

[12] R.D. Everett, G.G. Maul, HSV-1 IE protein Vmw110 causes redistribution of PML. EMBO J. 13 (21) (1994) 5062–5069.

[13] R.D. Everett, et al., Replication of ICP0-null mutant herpes simplex virus type 1 is restricted by both PML and Sp100, J. Virol. 82 (6) (2008) 2661–2672, https://doi.org/10.1128/JVI.02308-07.

[14] J. Prudden, et al., SUMO-targeted ubiquitin ligases in genome stability, EMBO J. 26 (August) (2007) 4089–4101, https://doi.org/10.1038/sj.emboj.7601838.

[15] C. Boutell, R.D. Everett, Regulation of alphaherpesvirus infections by the ICP0 family of proteins, J. Gen. Virol. 94 (PART3) (2013) 465–481, https://doi.org/10.1099/vir.0.048900-0.

[16] R.D. Everett, et al., Sequences related to SUMO interaction motifs in herpes simplex virus 1 protein ICP0 act cooperatively to stimulate virus infection, J. Virol. 88 (5) (2014) 2763–2774, https://doi.org/10.1128/JVI.03417-13.

[17] J. Song, et al., Identification of a SUMO-binding motif that recognizes SUMO-modified proteins, Proc. Natl. Acad. Sci. U.S.A. 101 (40) (2004) 14373–14378, https://doi.org/10.1073/pnas.0403498101.
[18] H. Li, et al., Chk2 is required for HSV-1 ICP0-mediated G2/M arrest and enhancement of virus growth, Virology 375 (1) (2008) 13–23, https://doi.org/10.1016/j.virol.2008.01.038.
[19] G. Dellaire, et al., Promyelocytic leukemia nuclear bodies behave as DNA damage sensors whose response to DNA double-strand breaks is regulated by NBS1 and the kinases ATM, Chk2, and ATR, J. Cell Biol. 175 (1) (2006) 55–66, https://doi.org/10.1083/jcb.200604009.
[20] Y. Xu, et al., Structural insight into SUMO chain recognition and manipulation by the ubiquitin ligase RNF4. Nat. Commun. 5 (May) (2014) 4217, https://doi.org/10.1038/ncomms5217.
[21] S. Tremblay-belzile, et al., Article structural and functional characterization of the phosphorylation-dependent interaction between PML and SUMO1, Structure 23 (2015) 126–138, https://doi.org/10.1016/j.str.2014.10.015.
[22] D.S. Wishart, B.D. Sykes, F.M. Richards, 'The chemical shift index: a fast and simple method for the assignment of protein secondary structure through NMR spectroscopy', Biochemistry 31 (6) (1992) 1647–1651, https://doi.org/10.1021/bi00121a010.
[23] C. Dominguez, R. Boelens, A.M.J.J. Bonvin, HADDOCK: a protein-protein docking approach based on biochemical or biophysical information, J. Am. Chem. Soc. 125 (7) (2003) 1731–1737, https://doi.org/10.1021/ja026939x.
[24] A.M. Sriramachandran, R.J. Dohmen, 'SUMO-targeted ubiquitin ligases', The Authors, Biochim. Biophys. Acta Mol. Cell Res. 1843 (1) (2014) 75–85, https://doi.org/10.1016/j.bbamcr.2013.08.022.
[25] P. Brand, T. Lenser, P. Hemmerich, Assembly dynamics of PML nuclear bodies in living cells, PMC Biophys. (2010), https://doi.org/10.1186/1757-5036-3-3.
[26] J.-S. Seeler, et al., Common properties of nuclear body protein SP100 and TIF1α chromatin factor: role of SUMO modification, Mol. Cell Biol. 21 (10) (2001) 3314, https://doi.org/10.1128/MCB.21.10.3314-3324.2001. LP – 3324.
[27] C.W. Tung, S.Y. Ho, Computational identification of ubiquitylation sites from protein sequences, BMC Bioinf. (2008), https://doi.org/10.1186/1471-2105-9-310.
[28] V. Akimov, et al., Ubisite approach for comprehensive mapping of lysine and n-terminal ubiquitination sites, Nat. Struct. Mol. Biol. (2018), https://doi.org/10.1038/s41594-018-0084-y.
[29] D.J. Davido, et al., Phosphorylation site mutations affect herpes simplex virus type 1 ICP0 function, J. Virol. 79 (2) (2005) 1232–1243, https://doi.org/10.1128/JVI.79.2.1232.
[30] C. Boutell, et al., Herpes simplex virus type 1 ICP0 phosphorylation mutants impair the E3 ubiquitin ligase activity of ICP0 in a cell type-dependent manner, J. Virol. 82 (21) (2008) 10647–10656, https://doi.org/10.1128/JVI.01063-08.
[31] H.H. Mostafa, et al., Herpes simplex virus 1 ICP0 phosphorylation site mutants are attenuated for viral replication and impaired for explant-induced reactivation, J. Virol. 85 (23) (2011) 12631–12637, https://doi.org/10.1128/JVI.05661-11.
[32] M.S. Chaurushiya, et al., 'Article viral E3 ubiquitin ligase-mediated degradation of a cellular E3: viral mimicry of a cellular phosphorylation mark targets the RNF8 FHA domain', Mol. Cell 46 (2012) 79–90, https://doi.org/10.1016/j.molcel.2012.02.004.
[33] M.C. Smith, et al., CK2 inhibitors increase the sensitivity of HSV-1 to interferon-β, Antivir. Res. 91 (3) (2011) 259–266, https://doi.org/10.1016/j.antiviral.2011.06.009.
[34] R.D. Everett, Interactions between DNA viruses, ND10 and the DNA damage response, Cell Microbiol. 8 (3) (2006) 365–374. CMI677 [pii]\r10.1111/j.1462-5822.2005.00677.x.
[35] C. Boutell, et al., A viral ubiquitin ligase has substrate preferential sumo targeted ubiquitin ligase activity that counteracts intrinsic antiviral defence, PLoS Pathog. 7 (9) (2011), https://doi.org/10.1371/journal.ppat.1002245.
[36] S. Muller, 'PML , SUMO , and RNF4: guardians', Mol. Cell 55 (2014) 1–3, https://doi.org/10.1016/j.molcel.2014.06.022.
[37] Y. Zheng, H. Gu, Identification of three redundant segments responsible for herpes simplex virus 1 ICP0 to fuse with ND10 nuclear bodies, J. Virol. 89 (8) (2015) 4214–4226, https://doi.org/10.1128/JVI.03658-14.
[38] Y. Zheng, S.K. Samrat, H. Gu, 'A tale of two PMLs : elements regulating a differential substrate recognition by the ICP0 E3 ubiquitin ligase of herpes simplex virus 1', J. Virol. 90 (23) (2016) 10875–10885, https://doi.org/10.1128/JVI.01636-16.
[39] H. Gu, Y. Zheng, 'Interaction of herpes simplex virus ICP0 with ND10 bodies: a sequential process of adhesion , fusion , and retention', J. Virol. 87 (18) (2013) 10244–10254, https://doi.org/10.1128/JVI.01487-13.
[40] W. Yue, E. Gershburg, J.S. Pagano, Hyperphosphorylation of EBNA2 by Epstein-Barr virus protein kinase suppresses transactivation of the LMP1 promoter, J. Virol. 79 (9) (2005) 5880–5885, https://doi.org/10.1128/JVI.79.9.5880-5885.2005.
[41] A. El-Guindy, et al., Phosphoacceptor site S173 in the regulatory domain of Epstein-Barr Virus ZEBRA protein is required for lytic DNA replication but not for activation of viral early genes. J. Virol. 81 (7) (2007) 3303–3316, https://doi.org/10.1128/JVI.02445-06.
[42] S.C. Kenney, J.E. Mertz, Regulation of the latent-lytic switch in Epstein-Barr virus, Semin. Canc. Biol. 26 (2014) 60–68, https://doi.org/10.1016/j.semcancer.2014.01.002.
[43] P. Purushothaman, T. Uppal, S.C. Verma, Molecular biology of KSHV lytic reactivation, Viruses 7 (1) (2015) 116–153, https://doi.org/10.3390/v7010116.
[44] T. Hunter, The age of crosstalk: phosphorylation, ubiquitination, and beyond, Mol. Cell 28 (5) (2007) 730–738, https://doi.org/10.1016/j.molcel.2007.11.019.
[45] J. Sheng, et al., Dissection of c-MOS degron, EMBO J. 21 (22) (2002) 6061–6071, https://doi.org/10.1093/emboj/cdf626.
[46] H. Dou, et al., Structural basis for autoinhibition and phosphorylation-dependent activation of c-Cbl. Nat. Struct. Mol. Biol. 19 (2) (2012) 184–192, https://doi.org/10.1038/nsmb.2231.
[47] C. Hoege, et al., RAD6-dependent DNA repair is linked to modification of PCNA by ubiquitin and SUMO, Nature 419 (6903) (2002) 135–141, https://doi.org/10.1038/nature00991.
[48] V. Hietakangas, et al., PDSM, a motif for phosphorylation-dependent SUMO modification, Proc. Natl. Acad. Sci. U.S.A. 103 (1) (2006) 45–50, https://doi.org/10.1073/pnas.0503698102.
[49] J. Bies, M. Sramko, L. Wolff, Stress-induced phosphorylation of Thr486 in c-Myb by p38 mitogen-activated protein kinases attenuates conjugation of SUMO-2/3, J. Biol. Chem. 288 (52) (2013) 36983–36993, https://doi.org/10.1074/jbc.M113.500264.

[50] C.C. Chang, et al., Structural and functional roles of daxx SIM phosphorylation in SUMO paralog-selective binding and apoptosis modulation, Elsevier Inc. Mol. Cell 42 (1) (2011) 62–74, https://doi.org/10.1016/j.molcel.2011.02.022.
[51] V. Tripathi, K.S. Chatterjee, R. Das, Casein kinase-2 mediated phosphorylation increases the SUMO-dependent activity of the cytomegalovirus transactivator IE2, J. Biol. Chem. (2019), https://doi.org/10.1074/jbc.RA119.009601.
[52] U. Knippschild, et al., The CK1 family: contribution to cellular stress response and its role in carcinogenesis, Front. Oncol. 4 MAY (May) (2014) 1–32, https://doi.org/10.3389/fonc.2014.00096.
[53] K.S. Chatterjee, V. Tripathi, R. Das, A conserved and buried edge-to-face aromatic interaction in small ubiquitin-like modifier (SUMO) has a role in SUMO stability and function, J. Biol. Chem. 294 (17) (2019) 6772–6784, https://doi.org/10.1074/jbc.RA118.006642.
[54] R. Das, et al., 'Allosteric regulation of E2:E3 interactions promote a processive ubiquitination machine, Nature Publishing Group, EMBO J. 32 (18) (2013) 2504–2516, https://doi.org/10.1038/emboj.2013.174.
[55] F. Delaglio, et al., NMRPipe: a multidimensional spectral processing system based on UNIX pipes, J. Biomol. NMR 6 (3) (1995) 277–293, https://doi.org/10.1007/BF00197809.
[56] D.G. Kneller, I.D. Kuntz, UCSF Sparky: an NMR display, annotation and assignment tool, J. Cell. Biochem. 53 (S17C) (1993) 254, https://doi.org/10.1002/jcb.240530709.
[57] S. Wiese, et al., Proteomics characterization of mouse kidney peroxisomes by tandem mass spectrometry and protein correlation profiling, Mol. Cell. Proteomics: MCP 6 (11) (2007) 2045–2057, https://doi.org/10.1074/mcp.M700169-MCP200.
[58] S.M. Brown, D.A. Ritchie, J.H. Subak-Sharpe, Genetic studies with herpes simplex virus type 1. The isolation of temperature-sensitive mutants, their arrangement into complementation groups and recombination analysis leading to a linkage map. J. Gen. Virol. 18 (3) (1973) 329–346, https://doi.org/10.1099/0022-1317-18-3-329.
[59] J.C. Phillips, et al., Scalable molecular dynamics with NAMD, J. Comput. Chem. (2005) 1781–1802, https://doi.org/10.1002/jcc.20289.
[60] A.D. MacKerell, M. Feig, C.L. Brooks, Improved treatment of the protein backbone in empirical force fields, J. Am. Chem. Soc. 126 (3) (2004) 698–699, https://doi.org/10.1021/ja036959e.
[61] J. Huang, A.D. Mackerell, CHARMM36 all-atom additive protein force field: Validation based on comparison to NMR data, J. Comput. Chem. 34 (25) (2013) 2135–2145, https://doi.org/10.1002/jcc.23354.
[62] J.P. Ryckaert, G. Ciccotti, H.J.C. Berendsen, Numerical integration of the cartesian equations of motion of a system with constraints: molecular dynamics of n-alkanes, J. Comput. Phys. 23 (3) (1977) 327–341, https://doi.org/10.1016/0021-9991(77)90098-5.
[63] J.P. Ryckaert, Special geometrical constraints in the molecular dynamics of chain molecules, Mol. Phys. 55 (3) (1985) 549–556, https://doi.org/10.1080/00268978500101531.
[64] U. Essmann, et al., A smooth particle mesh Ewald method, J. Chem. Phys. 103 (1995) (1995) 8577–8593, https://doi.org/10.1063/1.470117.
[65] G.J. Martyna, D.J. Tobias, M.L. Klein, Constant pressure molecular dynamics algorithms, J. Chem. Phys. 101 (September) (1994) 4177, https://doi.org/10.1063/1.467468.
[66] S.E. Feller, et al., Constant pressure molecular dynamics simulation: the Langevin piston method, J. Chem. Phys. 103 (11) (1995) 4613, https://doi.org/10.1063/1.470648.
[67] W. Humphrey, A. Dalke, K. Schulten, VMD-visual molecular dynamics, J. Mol. Graph. 14 (1996) 33–38, https://doi.org/10.1016/0263-7855(96)00018-5.
[68] E.F. Pettersen, et al., 'UCSF chimera—a visualization system for exploratory research and analysis', J. Comput. Chem. 25 (2004) 1605–1612, https://doi.org/10.1002/jcc.20084.